Accepted Manuscript

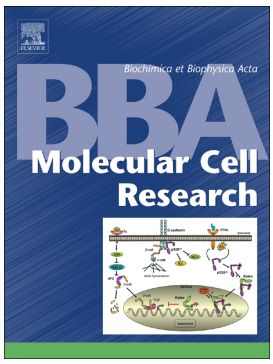

Dual knockdown of Galectin-8 and its glycosylated ligand, the activated leukocyte cell adhesion molecule (ALCAM/CD166), synergistically delays in vivo breast cancer growth

Fátima Ferragut, Alejandro J. Cagnoni, Lucas L. Colombo, Clara Sánchez Terrero, Carlota Wolfenstein-Todel, María F. Troncoso, Silvia I. Vanzulli, Gabriel A. Rabinovich, Karina V. Mariño, María T. Elola

PII: S0167-4889(19)30035-7
DOI: https://doi.org/10.1016/j.bbamcr.2019.03.010
Reference: BBAMCR 18463

To appear in: *BBA - Molecular Cell Research*

Received date: 18 October 2018
Revised date: 15 March 2019
Accepted date: 19 March 2019

Please cite this article as: F. Ferragut, A.J. Cagnoni, L.L. Colombo, et al., Dual knockdown of Galectin-8 and its glycosylated ligand, the activated leukocyte cell adhesion molecule (ALCAM/CD166), synergistically delays in vivo breast cancer growth, BBA - Molecular Cell Research, https://doi.org/10.1016/j.bbamcr.2019.03.010

This is a PDF file of an unedited manuscript that has been accepted for publication. As a service to our customers we are providing this early version of the manuscript. The manuscript will undergo copyediting, typesetting, and review of the resulting proof before it is published in its final form. Please note that during the production process errors may be discovered which could affect the content, and all legal disclaimers that apply to the journal pertain.

ACCEPTED MANUSCRIPT

Dual knockdown of Galectin-8 and its glycosylated ligand, the activated leukocyte cell adhesion molecule (ALCAM/CD166), synergistically delays *in vivo* breast cancer growth.

Fátima Ferragut[1], Alejandro J. Cagnoni[2], Lucas L. Colombo[3], Clara Sánchez Terrero[4], Carlota Wolfenstein-Todel[1], María F. Troncoso[1], Silvia I. Vanzulli[5], Gabriel A. Rabinovich[6,7], Karina V. Mariño[2], María T. Elola[1*].

[1] Instituto de Química y Fisicoquímica Biológicas Prof. Dr. Alejandro Paladini (CONICET-UBA). Facultad de Farmacia y Bioquímica. Universidad de Buenos Aires. Buenos Aires, Argentina.

[2] Laboratorio de Glicómica Funcional y Molecular, Instituto de Biología y Medicina Experimental (IBYME-CONICET). Buenos Aires, Argentina.

[3] Área de Investigación, Instituto de Oncología Ángel H. Roffo. Universidad de Buenos Aires. Buenos Aires, Argentina.

[4] Centro Oncológico de Medicina Nuclear, Comisión Nacional de Energía Atómica-Hospital Oncológico Ángel H. Roffo. Universidad de Buenos Aires. Buenos Aires, Argentina.

[5] Instituto de Investigaciones Hematológicas (IIHEMA), Academia Nacional de Medicina. Buenos Aires, Argentina.

[6] Laboratorio de Inmunopatología, Instituto de Biología y Medicina Experimental (IBYME-CONICET). Buenos Aires, Argentina.

[7] Departamento de Química Biológica, Facultad de Ciencias Exactas y Naturales. Universidad de Buenos Aires. Buenos Aires, Argentina.

[*] Correspondence: Dr. María Teresa Elola. Instituto de Química y Fisicoquímica Biológicas Prof. Dr. Alejandro Paladini (CONICET-UBA). Facultad de Farmacia y Bioquímica. Universidad de Buenos Aires. Junín 956 (C1113). Buenos Aires, Argentina. E-mail: mt_elola@yahoo.com. Phone: +54 11 52874122. Fax: +54 11 49625457.

ACCEPTED MANUSCRIPT

Abstract

Galectin-8 (Gal-8), a '*tandem-repeat'*-type galectin, has been described as a modulator of cellular functions including adhesion, spreading, growth arrest, apoptosis, pathogen recognition, autophagy, and immunomodulation. We have previously shown that activated leukocyte cell adhesion molecule (ALCAM), also known as CD166, serves as a receptor for endogenous Gal-8. ALCAM is a member of the immunoglobulin superfamily involved in cell-cell adhesion through homophilic (ALCAM-ALCAM) and heterophilic (*i.e.* ALCAM-CD6) interactions in different tissues. Here we investigated the physiologic relevance of ALCAM-Gal-8 association and glycosylation-dependent mechanisms governing these interactions. We found that silencing of ALCAM in MDA-MB-231 triple negative breast cancer cells decreases cell adhesion and migration onto Gal-8-coated surfaces in a glycan-dependent fashion. Remarkably, either Gal-8 or ALCAM silencing also disrupted cell-cell adhesion, and led to reduced tumor growth in a murine model of triple negative breast cancer. Moreover, structural characterization of endogenous ALCAM N-glycosylation showed abundant permissive structures for Gal-8 binding. Importantly, we also found that cell sialylation controls Gal-8-mediated cell adhesion. Altogether, these findings demonstrate a central role of either ALCAM or Gal-8 (or both) in controlling triple negative breast cancer.

Key words: ALCAM (CD166) / Galectin-8 / triple negative breast cancer / cell adhesion and migration / tumor growth / sialylation / N-glycosylation

Running title: Dual Gal-8 and ALCAM silencing delays tumor growth

ACCEPTED MANUSCRIPT

ACCEPTED MANUSCRIPT

1. Introduction

Galectin-8 (Gal-8), an endogenous "*tandem-repeat*"-type galectin [1,2] with two carbohydrate recognition domains (CRDs), shows a complex gene regulation, and presents at least seven isoforms as a result of mRNA splicing [3,4]. Gal-8 has been described as a modulator of different cellular functions including cell adhesion and spreading [5-7], growth arrest and apoptosis [8], pathogen recognition [9], autophagy [10,11], and immunosuppression [12]. Gal-8 is one of the most widely expressed "*tandem-repeat*" galectins in human tissues, being detected in normal and tumor cells [13-16]. Of note, the level of amplification of *LGALS8* (Gal-8 gene) in different cancer patients exceeds by far that of other common galectins like Gal-1 or Gal-3, particularly in breast tumors [17]. In breast cancer, and using validated and clinically relevant genetically engineered mouse models (GEMMs), Gal-8 was shown to be one of the five most frequently identified genes among fifteen tumor antigens detected in a *neu* transgenic mouse model with negative estrogen receptor [18]. Moreover, in sera from patients with breast cancer, Gal-8 concentrations were higher than in healthy individuals [19,20]. Importantly, Gal-8 overexpression has been shown to transform MDCK canine kidney cells, inducing reversible epithelial-mesenchymal transition (EMT), and leading to larger tumors than parental cells when subcutaneously inoculated in immunosuppressed mice [21].

Upon secretion, Gal-8 has been shown to act as a matrix protein equipotent to fibronectin in the promotion of cell adhesion, by ligating and inducing clustering of several cell surface receptors, *i.e.* integrins [4-6,22]. For example, immobilized Gal-8 supported dose-dependent cell adhesion of H1299 human non-small cell lung carcinoma cells, Fao rat hepatoma cells, HeLa human cervical cancer cells, NIH-hIR murine fibroblasts as well as CHO-P Chinese hamster ovary [6,23] and human trabecular meshwork cells [24]. In glioblastoma cells, immobilized Gal-8 promoted U373 cell migration [25], while soluble Gal-8, acting as a chemoattractant, induced the migration of U87 cells [26]. Accordingly, binding of metastatic lung cancer cells to Gal-8 in combination with fibronectin has been associated with the metastatic progression of lung adenocarcinoma [27]. Moreover, Gal-8 also promoted lymphatic endothelial cell adhesion and migration [28], and vascular endothelial cell migration [29]. Notably, Gal-8 has been reported to induce increased adhesion of colon cancer cells to endothelial cells [19,30], suggesting that moderate concentrations of Gal-8 in serum might favour dissemination of tumor cells by promoting their heterotypic adhesion to vascular or lymphatic endothelium. Noteworthy, and in addition to its role in cell adhesion and migration, Gal-8 plays key roles in angiogenesis [29,31],

ACCEPTED MANUSCRIPT

osteolysis [32,33], and may also influence tumor-immune escape as it promotes expansion of regulatory T cells through modulation of TGF-β and IL-2 signaling [12].

We have previously shown that activated leukocyte cell adhesion molecule (ALCAM/ CD166) serves as a receptor for endogenous Gal-8 in endothelial cells [29]. ALCAM, a member of the immunoglobulin superfamily with five extracellular immunoglobulin-like domains, functions as a cell-cell adhesion modulator in homophilic (ALCAM-ALCAM) and heterophilic (*i.e.* ALCAM-CD6) interactions in different tissues [34-36]. With respect to ALCAM in murine tumor models, Hansen *et al.* reported ALCAM detection in histological sections of xenografted tumors derived from MDA-MB-231 breast cancer cells by immunofluorescence staining, although the effects of ALCAM targeting on tumorigenesis were not evaluated [37]. Remarkably, ALCAM knockdown induced a reduction in tumor cell growth as compared to controls in mouse models of endometrial and pancreatic cancer as well as hepatocellular carcinoma [38-42].

In a previous study [20], we have found that ALCAM-silenced breast cancer cells displayed reduced binding to immobilized Gal-8 relative to control cells. Importantly, our studies also highlighted that extracellular Gal-8 promoted receptor segregation, probably trapping ALCAM at the surface of breast cancer cells [20]. When analyzing ALCAM-Gal-8 interactions by surface plasmon resonance (SPR), we were able to prove that this lectin recognizes its ligand in a glycan-dependent manner [20]. In this regard, as observed with other "*tandem-repeat*" type galectins [43-45], full-length Gal-8 presents a broader specificity for *N*-acetyllactosamine derivatives when compared to each of its CRDs separately: while Gal-8 N-CRD (Gal-8N) exhibits marked preference for α(2-3)-sialylated or 3-sulfated β-galactosides [43-47], Gal-8C shows preferential recognition for A- or B-blood group structures. As a consequence, full-length Gal-8 is able to elicit particular effects on the cell surface by synergistic action of both CRDs, involving interactions with high density ligands of moderate affinity for each isolated CRD [45].

Herein, we investigated the physiologic relevance of ALCAM-Gal-8 interactions in breast cancer cells. We found that ALCAM knockdown in MDA-MB-231 breast cancer cells decreases cell adhesion and migration onto Gal-8 surfaces in a glycan-dependent fashion. Moreover, silencing of Gal-8 or ALCAM prevented cell-cell adhesion, whereas dual silencing synergistically delayed *in vivo* tumor growth. Detailed structural N-glycoprofiling of ALCAM purified from MDA-MB-231 breast cancer cells revealed the presence of abundant permissive structures for Gal-8 binding. Furthermore, our results showed that cell sialylation modulates adhesion of MDA-MB-231 cells to Gal-8-coated surfaces. Altogether, these findings

ACCEPTED MANUSCRIPT

demonstrate a central role of either ALCAM or Gal-8 (or both) in controlling triple negative breast cancer.

2. Materials and methods

2.1. Reagents

Polyvinylidene-difluoride (PVDF) membranes and Affi-Gel 10 were obtained from Bio Rad (Hercules, CA, USA). Anti-rabbit IgG conjugated to horseradish peroxidase (HRP), anti-β-actin, lactose, sucrose, aprotinin, sodium pyrophosphate, L-glutamine, 3-[4,5-dimethylthiazol-2-yl]-2,5-diphenyltetrazolium bromide (MTT), saponin, paraformaldehyde, bovine serum albumin (BSA), and phenylmethylsulfonyl fluoride (PMSF) were obtained from Sigma-Aldrich (St. Louis, MO, USA). The monoclonal anti-Gal-8 antibody was purchased from Abcam (Cambridge, MA, USA). The anti-ALCAM monoclonal antibody (clone MOG/07, NCL-CD166) was obtained from Novocastra-Leica (Newcastle, UK); anti-ALCAM monoclonal antibody from Abcam (clone 3A6) was also used. Dulbecco's modified Eagle's medium, streptomycin/penicillin, 4',6-diamidino-2-phenylindole (DAPI), Alexa Fluor 488-conjugated secondary antibody (Molecular Probes), matrigel Geltrex (growth factor-reduced) and recombinant human ALCAM were obtained from Invitrogen Life Technologies (Carlsbad, CA, USA). Fetal bovine serum (FBS) was purchased from Natocor (Villa Carlos Paz, Córdoba, Argentina). Diazabicyclo[2.2.2]octane (DABCO) was obtained from Fluka (Steinheim, Germany). Alexa Fluor 555-conjugated and HRP-conjugated anti-mouse IgG were purchased from Cell Signaling (Danvers, MA, USA). Pierce ECL Plus Western Blotting substrate was purchased from Thermo Fisher Scientific (Waltham, MA, USA). *Maackia amurensis* II (MAL II) and *Sambucus nigra* agglutinin (SNA) plant lectins were obtained from Vector Laboratories (Burlingame, CA, USA).

2.2. Cell lines, constructs and generation of cell lines

MDA-MB-231 (ATCC HTB-26) breast cancer cells were cultured in Dulbecco's modified Eagle's medium containing 25 mM glucose, supplemented with 10% heat-inactivated fetal bovine serum (FBS), 2 mM L-glutamine, 100 μg/ml streptomycin and 100 units/ml penicillin. Cells were detached from the plates with EDTA (0.53 mM EDTA, 140 mM NaCl, 5.4 mM KCl, 5.5 mM glucose, pH 7.2). To establish MDA-MB-231 cell lines in which Gal-8 expression was stably knocked-down, cells were transduced with specific shRNA lentiviral particles (sc-37429-V, Santa Cruz Biotechnology), following the manufacturer´s instructions. To establish MDA-MB-231 cell lines in which ALCAM/CD166 expression was stably knocked-down, cells were transduced with

ACCEPTED MANUSCRIPT

ALCAM-specific shRNA lentiviral particles (sc-43023-V, Santa Cruz Biotechnology). Control lentivirus (sc-108080, Santa Cruz Biotechnology), carrying scrambled-shRNA, was used for mock transduction. Finally, cells were selected in 1 μg/ml puromycin, Gal-8 and ALCAM expression were evaluated by Western blot, and knocked-down or mock-transduced cells were cultured and maintained in 1 μg/ml puromycin-containing culture medium. For analysis of Gal-8 secretion, subconfluent cell monolayers were cultured with or without FBS for 24-48 h, and then conditioned media were collected and centrifuged for 10 min at 400 *x g*; sodium dodecyl sulfate (SDS) was added to the supernatants to a 0.5% (w/v) final concentration, then heated at 100 °C for 10 min, and diluted with 1:10 methanol, followed by a -20 °C overnight incubation; after centrifugation at 21,000 *x g* for 30 min, pellets were recovered and protein concentration was determined.

2.3. Western blot analysis

Cells were homogenized in lysis buffer (100 mM Tris, pH 7.4, 1% v/v Triton X-100, 10 mM EDTA, 100 mM sodium pyrophosphate, 4 mM PMSF). Cell lysates were centrifuged for 10 min at 12,000 *x g* at 4 ºC, supernatants were collected and protein concentration was determined. Samples from cell lysates or conditioned media (30 μg of protein/lane) were separated by SDS-PAGE, and then electrotransferred onto PVDF membranes. Blots were probed with the primary antibodies overnight at 4 ºC. Detection of β-actin with anti-β-actin antibody was used to normalize protein loading in cell lysates. After incubating with the corresponding HRP-conjugated secondary antibodies, immunoreactive bands were detected by chemiluminiscence. Densitometric analysis of protein levels was performed using *Image J* software (U.S. National Institutes of Health, Bethesda, MD, US; http://rbsweb.nih.gov/ij/).

2.4. Cell adhesion assay

Recombinant full-length Gal-8 (medium Gal-8 or M isoform; rGal-8) was prepared as previously reported [20,29]. Tissue culture plates (96-wells) were coated with rGal-8 (0.25-3 μM) or BSA (0.1% w/v) overnight at 4 °C, and blocked with BSA (0.1% w/v) for 1 h at room temperature. Cells were detached from the plates with EDTA, washed with PBS, resuspended in FBS-free medium, and 2-3 x 10^4 cells/well were seeded onto the coated plates incubating for 1-2 h at 37 ºC. Afterwards, cells were washed, fixed in 4% paraformaldehyde and stained with 0.5% crystal violet in acetic acid 3% (v/v) for 20 min at room temperature. Excess dye was removed by three washes with water, and cells were solubilized in 1% SDS (w/v) at room temperature for 1 h. Cell binding was quantified by measuring the absorbance at 595 nm in a microplate reader Biotrak II

ACCEPTED MANUSCRIPT

(Amersham Bioscience-GE Healthcare, Buckinghamshire, UK). Specific binding was defined as the difference between the absorbance of cells binding to rGal-8-coated wells and the absorbance of cells binding to BSA-coated wells. All assays were performed in triplicate. When indicated, coating was performed after incubating rGal-8 (2 μM) with disaccharides such as lactose (100 mM) or sucrose (100 mM) at room temperature for 30 min.

2.5. Indirect immunofluorescence

Cells were grown on uncoated coverslips in 24-well plates for 48 h. Cells were then rinsed twice in cold PBS and fixed in 4% paraformaldehyde at 0 ºC for 30 min. After washing, cells were blocked in 5% heat-inactivated human serum; when indicated, permeabilization was performed in 0.05% saponin in PBS for 1 h. Staining for ALCAM was performed by incubating with an anti-ALCAM monoclonal antibody overnight at 4 ºC, followed by Alexa Fluor 555-conjugated secondary antibody for 1 h at room temperature. Negative controls were performed by substituting the primary antibody by PBS, followed by the corresponding secondary antibody. Nuclei were stained with DAPI. Samples were mounted in DABCO and observed under a Fluo View FV1000 confocal microscope (Olympus, Tokyo, Japan).

2.6. Scratch wound assay

Migration was evaluated by means of the scratch wound assay. Thus, 1 x 10^4 cells/well were seeded onto 96-well plates, containing different concentrations of full-length rGal-8 (2 μM). Cells were allowed to grow to confluence in DMEM in the presence of 10% FBS for 48 h. Finally, a scratch was performed using a 20-μl tip, and cells were washed twice with PBS and incubated with DMEM without FBS for 20 h at 37 ºC. Cells were photographed and *Image J* software was used to determine the whole area of the wound at 20 h versus 0 h (wound closure (%) = [area at 20 h / area at 0 h x 100]). When indicated, pre-coating was performed after incubating the lectin with disaccharides such as lactose (100 mM) or sucrose (100 mM) at room temperature for 30 min.

2.7. Cell aggregation assay

To analyze cell-cell interactions, single-cell suspensions were prepared, and 5 x 10^3 cells/sample were incubated in FBS-free DMEM with gentle rotation (80 rpm) at 37 °C for 1 h, in microfuge tubes. Then, each sample was loaded onto different wells of 96-well plates to be photographed. The number of free cells was counted at 0 and 1 h in five fields/sample. The percentages of free cells were calculated for individual samples (free cells (%) = [number of free cells at 1 h / number

ACCEPTED MANUSCRIPT

of free cells at 0 h x 100]), and each assay was performed in triplicates. When indicated, aggregation was performed adding soluble rGal-8 (1-5 μM). To determine if the aggregation process was carbohydrate-dependent, cells were incubated with rGal-8 (2 μM) and disaccharides (lactose as a competitor for Gal-8 binding, and sucrose as a negative control, 100 mM).

2.8. Cell proliferation

Measurements of cell viability were determined using the 3-[4,5-dimethylthiazol-2-yl]-2,5-diphenyltetrazolium bromide (MTT) assay. Briefly, 0.3 x 10^4 cells/well were plated in 96-well plates in DMEM plus 10% FBS, and allowed to attach for 24 h at 37 ºC. Then, cells were incubated in FBS-free DMEM for 24 h at 37 ºC. Afterwards, cells were incubated in DMEM containing 10% FBS, and cell proliferation was measured after 0, 24, 48, 72 and 96 h. Briefly, at any indicated time, 20 μl of MTT solution (4 mg/ml) was added to each well, and the plates were incubated for an additional 2 h at 37 ºC. In order to solubilize the formazan crystals formed in viable cells, dimethyl sulfoxide (150 μl) was added to each well, before measuring the absorbance at 595 nm.

2.9. Colony formation

To evaluate the ability of single cells to form colonies, 0.3 x 10^3 cells/well were loaded in 24-well plates in DMEM with 10% FBS. Cells were incubated for 10 days at 37 °C, and culture medium was replaced every 3 days. Afterwards, cells were washed, fixed in 4% paraformaldehyde and stained with 0.5% crystal violet in acetic acid 3% (v/v) for 20 min at room temperature. Colonies were photographed and quantified under a light microscope.

2.10. Spheroid-formation assay

Fifty microliters of matrigel Geltrex/well were loaded into 96-well plates, which were incubated for 2 h at 37 °C. Cells were seeded onto matrigel at a density of 1 x 10^4 cells/well in DMEM plus 10% FBS. Culture medium was replaced every 3 days. After 10 days at 37 °C, spheroids were photographed under a light microscope. Each assay was performed in triplicates. Spheroids were photographed in five fields/sample, and their volumes were measured using *Image J* software, applying the formula: [volume (mm^3) = 4/3 π r^3], where r is the sphere radius.

2.11. Xenograft murine model

ACCEPTED MANUSCRIPT

Animal care and manipulation were performed in agreement with the National Institutes of Health guide for the care and use of laboratory animals (NIH Publications Number 8023, revised 1978). The Ethical Committee from Instituto de Oncología Angel H. Roffo approved the experiments and the use of animals for this work, according to the institutional guidelines for animal welfare. Eight-week-old female athymic *nude* mice (Comisión Nacional de Energía Atómica, Ezeiza, Buenos Aires, Argentina) were subcutaneously inoculated with tumor cells. Each mouse was injected with 10^7 cells/50 µl of PBS plus 50 µl of matrigel Geltrex, and each group of animals was composed of 5-6 mice. When tumors were palpable, sizes were measured with a Vernier caliper 2-3 times a week. Tumor volume was calculated with each radius (r_1, r_2 and r_3), applying the formula: [volume (mm^3) = 4/3 π r_1 r_2 r_3]. Growth curves were performed plotting tumor volume versus time. Mice were sacrificed at 56 or 98 days after injection. Tumor growth and dissemination were evaluated macroscopically *ex vivo*. For histological analysis, all extracted tissues (tumors and lymph nodes) were fixed in 10% neutral buffered formalin, stained with haematoxylin and eosin, and evaluated by a pathologist.

2.12. N-Glycoprofiling of endogenous ALCAM from MDA-MB-231 cells

ALCAM from MDA-MB-231 cells was purified by affinity chromatography in a rGal-8-Affi-Gel 10 column as previously described [20,29]. After blotting onto PVDF membranes, this glycoprotein was identified by Western blot, and de-N-glycosylated using peptide N-glycosidase F (1,000 U/ml; Roche, Manheim, Germany) for 16 h in 20 mM $NaHCO_3$ buffer (37 ºC) [48]. Then, the digested N-glycans were separated by filtration (Nanosep 10K Omega, Pall Life Sciences, New York, NY, USA) and subsequently labelled with 2-aminobenzamide (2AB) by reductive amination. Excess of 2AB was removed by paper chromatography [49], or by LudgerClean S Cartridges (Ludger Ltd., Oxford, UK). Then, 2AB-labelled N-glycans were separated by ultra-performance hydrophilic interaction liquid chromatography (HILIC) with fluorescence detection (FLR λ_{ex} = 330 nm, λ_{em} = 420 nm) using a BEH Glycan column (150 x 2.1 mm, 1.7 µm bridged ethylsiloxane/silica hybrid particles, Waters, Milford, MA, USA) on an Acquity H-Class instrument (Waters, Milford, MA, USA). Solvent A was 50 mM formic acid adjusted to pH 4.4 with ammonia solution. Solvent B was acetonitrile. The column temperature was set to 40 °C. The 30 min method was used with a linear gradient of 30−47% with buffer A at 0.56 mL/min flow rate for 23 min followed by 47−70% A and finally reverting back to 30% A to complete the run method [50]. The injection volume was 10 µl, and samples were prepared in 70% (v/v) acetonitrile and stored at 5 ºC before injection. A dextran hydrolysate ladder was used to convert retention times into glucose unit (GU) values. All the data were processed using the

ACCEPTED MANUSCRIPT

Waters Empower 3 chromatography workstation software. Structural analysis of the released N-glycans was assisted by digestion with exoglycosidases [51], including: α(1-3,4)-fucosidase (cloned from sweet almond tree and expressed in *Pichia pastoris*); α(2-3,6,8,9) neuraminidase A (cloned from *Arthrobacter ureafaciens* and expressed in *E. coli*); α(2-3) neuraminidase and β(1-4)-galactosidase (both cloned from *Streptococcus pneumoniae* and expressed in *E. coli*); α(1-2,3)-mannosidase (cloned from *Xanthomonas manihotis* and expressed in *E. coli*). Enzymatic digestions were performed on 2AB-labelled N-glycans in manufacturer's recommended buffers for 16 h at 37 ºC. After digestion, N-glycans were separated from exoglycosidases before chromatographic analysis by centrifugation in a Nanosep 10K Omega microcentrifuge filter (Pall Life Sciences, New York, USA). All exoglycosidases were purchased from New England Biolabs (Massachussets, USA).

For sialylation analysis, separation of neutral and acidic oligosaccharides was performed by Weak Anion Exchange (WAX) chromatography (WAX-HPLC) using a BioSuite DEAE 2.5 μm NP AXC 4.6 x 35 mm column (Waters, Milford, MA, USA). Solvent A was ammonium acetate 50 mM (pH 7.0) in 20% v/v acetonitrile, and solvent B was 20% v/v aqueous acetonitrile. Gradient conditions were as follows: an initial equilibration of 2 min of 0% A, a linear gradient of 0 to 40% A over 4 min at a flow rate of 0.5 ml/min, followed by 40 to 100% A over 3 min, then 4 min at 100% A, 100 to 0% A over 0.5 min, and then 3.5 min at 0% A. Samples (10 μL) were injected in water and fluorescently-labelled fetuin N-glycans were used as a reference [50]. As both sialylation and sulfation can provide negative charge to 2AB-labelled N-glycans, digestion with α(2-3,6,8,9) neuraminidase A was performed to confirm absence of sulfated structures. Percentage of α(2-3) sialic acid was determined by specific cleavage with α(2-3) neuraminidase.

2.13. Characterization of cell surface sialylation by flow cytometry

MDA-MB-231 cells (1 x 10^6) were washed three times in PBS, and incubated in 250 μl of DMEM FBS-free containing either 20 U α(2-3,6,8,9) neuraminidase A or 40 U α(2-3) neuraminidase at 37 ºC for 2 h. After washing, cell sialylation was evaluated by flow cytometry using biotin-conjugated plant lectins including *Maackia amurensis* II (MAL II), which recognizes α(2-3)- sialylated structures (10 μg/ml), and *Sambucus nigra* agglutinin (SNA), which recognizes α(2-6)-sialylated glycans (5 μg/ml). In brief, unspecific interactions with plant lectins were avoided by washing in 1% BSA-PBS, and incubating cells with biotin-conjugated MAL II and SNA in 1% BSA, 10 mM HEPES, 150 mM NaCl, pH 7.4 on ice for 1 h. After washing, cells were incubated with phycoerythrin (PE)-conjugated streptavidin (ThermoFisher) on ice for 1 h.

ACCEPTED MANUSCRIPT

Cells were then washed, fixed in 4% paraformaldehyde, and analyzed by flow cytometry in a PASS III flow cytometer (Partec, Görlitz, Germany). Twenty thousand events were acquired for each sample, and data analysis was performed using FlowJo LLC (Ashland, Oregon, USA) software program.

2.14. Statistical analysis

Data were analyzed using GraphPad Prism 6.01 Software (GraphPad Software Inc., La Jolla, CA, US) and results are expressed as the mean ± standard error of the mean (S.E.M.) from, at least, three independent experiments. Differences between groups were assessed by one-way analysis of the variance (ANOVA) or two-way ANOVA (with appropriate post-tests). Values of $p<0.05$ were considered statistically significant.

3. Results

3.1 Silencing ALCAM in MDA-MB-231 breast cancer cells decreases cell adhesion and migration onto Gal-8-coated plates

To understand the role of Gal-8 and ALCAM in breast cancer cell interactions and motility, we silenced both Gal-8 and ALCAM in MDA-MB-231 cells. Cells were transduced with ALCAM-specific shRNA lentiviral particles (MDA-shALCAM) or Gal-8-specific shRNA lentiviral particles (MDA-shGal8), while control cells were transduced with scrambled-shRNA lentiviral particles (mock-transduced; MDA-shControl). Gal-8 knockdown (Fig. 1A) in MDA-shGal8 cells rendered approximately 50% reduction in protein expression, while ALCAM knockdown (Fig. 1B) in MDA-shALCAM showed 80% decrease in protein level, as determined in both cases against MDA-shControl by Western blot. Finally, a Gal-8- and ALCAM-double-silenced cell line (MDA-shALCAM-shGal8) was generated, obtaining 50% and 80% of Gal-8 (Fig. 1A) and ALCAM (Fig. 1B) silencing, respectively.

To analyze interactions between MDA-MB-231 cell surface ALCAM and Gal-8, we evaluated cell adhesion using full-length rGal-8-coated plates. We observed enhanced cell adhesion with increasing rGal-8 concentrations (0.25-3 μM) for all cell lines analyzed (Fig. 1C). MDA-shALCAM and MDA-shALCAM-shGal8 cells, which exhibited low levels of surface ALCAM (Fig. 1D), showed significantly reduced adhesion to rGal-8-coated plates ($p<0.05$) compared to MDA-MB-231, MDA-shControl or MDA-shGal8 cells (Fig. 1C), highlighting the relevance of interactions between endogenous ALCAM and extracellular Gal-8 in tumor cell adhesion. No significant differences were observed between MDA-shALCAM and MDA-

ACCEPTED MANUSCRIPT

shALCAM-shGal8 cell adhesion on rGal-8-coated plates (1-3 μM). Similarly, no significant differences in cell adhesion on rGal-8-coated plates were observed between MDA-MB-231, MDA-shControl or MDA-shGal8 cells (Fig. 1C). Remarkably, cell adhesion on rGal-8-coated plates (2 μM) was shown to be carbohydrate-dependent as 100 mM lactose, a galectin-specific ligand, was able to inhibit adhesion in the three ALCAM$^+$ (MDA-MB-231, $p<0.05$; MDA-shControl, $p<0.05$; MDA-shGal8, $p<0.05$) cell lines, whereas sucrose (100 mM) -a non-specific disaccharide- did not show any effect (Fig. 1E). Interestingly, in ALCAM-silenced cell lines (MDA-shALCAM and MDA-shALCAM-shGal8 cells), adhesion on rGal-8-coated plates was not significantly reduced by lactose. In conclusion, ALCAM silencing in MDA-MB-231 cells decreases *in vitro* cell binding to rGal-8, and the ALCAM-Gal-8 interactions are -at least partially- glycan-mediated. Although other cell surface Gal-8 ligands could also be involved in cell adhesion, such as integrins [5,6,22], these results suggest a main role for glycan-dependent ALCAM-Gal-8 interactions operating at the surface of MDA-MB-231 cells.

In 2D wound healing assays, ALCAM silencing decreased the wound closure rate of MDA-MB-231 cells onto rGal-8-coated (2 μM) surfaces (Fig. 2). ALCAM$^+$ cell lines (MDA-MB-231, MDA-shControl and MDA-shGal8 cells) migrated significantly faster ($p<0.001$) onto rGal-8 than ALCAM-silenced (MDA-shALCAM and MDA-shALCAM-shGal8) cells after 20 h (Fig. 2A, B). Moreover, MDA-MB-231, MDA-shControl or MDA-shGal8 cells (ALCAM$^+$ cells) showed significantly enhanced cell migration onto rGal-8-coated plates when compared to uncoated wells ($p<0.001$, $p<0.01$ and $p<0.01$, respectively; Fig. 2A, B). Conversely, ALCAM-silenced cell lines showed a trend towards an increased migration onto rGal-8-coated plates versus uncoated surfaces, which did not reach statistical significance (Fig. 2A, B). Hence, the stimulatory effect of rGal-8 on cell migration was only significant in ALCAM$^+$ cell lines, thus indicating a role for surface ALCAM-extracellular Gal-8 interactions on breast cancer cell migration. In the case of uncoated culture plates, while Gal-8 silencing did not modify the rate of migration in MDA-MB-231 cells, ALCAM silencing did significantly reduce ($p<0.001$) cell motility (Fig. 2A, B). Importantly, cell migration onto rGal-8-coated surfaces was markedly inhibited by lactose (10.12±1.78%) in the three ALCAM$^+$ (MDA-MB-231, $p<0.001$; MDA-shControl, $p<0.01$; MDA-shGal8, $p<0.01$) cell lines (Fig. 2C, D), but not by the unrelated disaccharide sucrose (Fig. 2C, D). In contrast, in ALCAM-silenced (MDA-shALCAM and MDA-shALCAM-shGal8) cells, migration onto rGal-8-coated wells was not significantly reduced by lactose (4.95±0.35%), suggesting a main role for glycan-dependent ALCAM-Gal-8 interactions in mediating migration of MDA-MB-231 cells (Fig. 2C, D). In conclusion, ALCAM silencing in

ACCEPTED MANUSCRIPT

MDA-MB-231 cells decreases *in vitro* cell migration both onto rGal-8-coated surfaces and onto uncoated culture plates. Importantly, a favourable glycan-mediated effect of rGal-8, acting as a matricellular ligand, is observed on the motility of $ALCAM^+$ cells, which is abrogated by ALCAM knockdown, highlighting the relevance of glycan-dependent ALCAM-Gal-8 interactions at the surface of MDA-MB-231 cells.

3.2 Silencing of Gal-8 and ALCAM in MDA-MB-231 breast cancer cells decreases cell-cell adhesion in a 3D model

To mimic *in vitro* tumor progression, we used a 3D model to study the formation of cell aggregates. Thus, we developed a cell aggregation assay and quantitatively determined Gal-8 and ALCAM effects in cell-cell adhesion. Gal-8 silencing markedly inhibited cell aggregation in MDA-MB-231 cells: notably, MDA-shGal8 cells exhibited significantly increased percentage of free cells ($p<0.05$) when compared to MDA-shControl cells after 1 h of cell-cell adhesion (Fig. 3A, B). Similarly, ALCAM-silenced tumor cells showed significantly reduced ($p<0.05$) cell-cell adhesion as compared to MDA-shControl cells (Fig. 3A, B).

Exogenously-added soluble rGal-8 (1 μM) rendered a significant increase in cell aggregation in Gal-8-silenced cells (MDA-shGal8 cells, $p<0.001$; MDA-shALCAM-shGal8 cells, $p<0.05$) (data not shown), demonstrating the role of secreted Gal-8 in cell-cell interactions in the extracellular milieu. In control MDA-MB-231 and MDA-shControl cells, increasing concentrations of exogenous soluble rGal-8 (2-5 μM) significantly increased aggregation in a glycan-dependent manner (Fig. S1).

In conclusion, either Gal-8 or ALCAM silencing attenuates cell-cell aggregation, although dual silencing does not produce any enhanced effect.

3.3 ALCAM silencing inhibits cell proliferation in MDA-MB-231 breast cancer cells

Next, we examined whether ALCAM or Gal-8 may also affect cell proliferation of MDA-MB-231 cells (Fig. 4A). After 72 hour incubation, MDA-shALCAM-shGal8 cells showed decreased proliferation compared to MDA-MB-231 ($p<0.05$), MDA-shControl ($p<0.01$) and MDA-shGal8 ($p<0.05$) cells, as measured by colorimetric MTT-based assay. Interestingly, at 96 h, both MDA-shALCAM ($p<0.05$; $p<0.01$) and MDA-shALCAM-shGal8 ($p<0.001$; $p<0.001$) cells showed decreased proliferation compared to control MDA-MB-231 and MDA-shControl cells, respectively. MDA-shALCAM ($p<0.01$) and MDA-shALCAM-shGal8 ($p<0.001$) cells also showed decreased proliferation compared to MDA-shGal8 cells. There were no statistical

ACCEPTED MANUSCRIPT

differences between ALCAM$^+$ cell lines or between ALCAM-silenced cell lines at 72 or 96 h (Fig. 4A), indicating that ALCAM silencing -but not Gal-8 silencing- decreased MDA-MB-231 cell proliferation. Furthermore, we found that ALCAM-silenced cells showed impaired ability to form anchorage-dependent colonies (p<0.001) compared to ALCAM$^+$ cells (MDA-MB-231, MDA-shControl and MDA-shGal8 cells) (Fig. 4B). Accordingly, when we evaluated spheroid formation after 10 days, ALCAM-silenced cells produced spheres with significantly reduced volumes (p<0.001) compared to those derived from ALCAM$^+$ cells (Fig. 4C). We conclude that ALCAM silencing reduces MDA-MB-231 cell ability to form colonies and spheroids, which is probably related to the effects of ALCAM silencing on cell proliferation. Thus, ALCAM is involved in cell growth and survival of human MDA-MB-231 breast cancer cells.

3.5 Silencing ALCAM and Gal-8 affects primary tumor growth in a murine model of triple negative breast cancer

To analyze the effect of Gal-8 and ALCAM on tumor development and metastasis, we subcutaneously inoculated human MDA-MB-231 breast tumor cells in athymic *nude* mice. At day 56 *post-inoculum* (*p.i.*), MDA-shGal8 cells generated smaller tumors (p<0.05) than control MDA-MB-231 and MDA-shControl cells (Fig. 5A, B). Tumors developed from control MDA-shControl cells did not show any significant difference in volume as compared to those derived from MDA-MB-231 control cells at any time evaluated (Fig. 5 A, B). Control mice as well as mice inoculated with MDA-shGal8 cells were euthanized because of ethical reasons at day 56 *p.i.* to allow the comparisons between groups. ALCAM-silenced cells developed very small tumors after 56 days of injection (p<0.01) as compared to tumors derived from control MDA-MB-231 and MDA-shControl cells (Fig. 5 A, B). Moreover, at day 56 *p.i.*, mice inoculated with MDA-shALCAM and MDA-shALCAM-shGal8 cells developed significantly smaller tumors (p<0.05) than those inoculated with MDA-shGal8 cells (Fig. 5 A, B). Mice injected with MDA-shALCAM and MDA-shALCAM-shGal8 cells were kept alive to monitor potential growth differences between experimental groups. Notably, at day 98 *p.i.*, we observed that tumors generated by MDA-shALCAM-shGal8 cells were smaller (p<0.05) than those generated by MDA-shALCAM cells (Fig. 5A). In summary, dual silencing of Gal-8 and ALCAM induced a significant delay on tumor growth, even more pronounced as that observed following Gal-8 or ALCAM silencing alone. In order to evaluate if Gal-8 and ALCAM were still efficiently downregulated in primary tumors developed in different groups, Western blot analysis was performed after tumor resection. Tumors derived from MDA-shGal8 cells showed significantly decreased Gal-8 protein levels at day 56 *p.i.* (p<0.01) compared to tumors generated by control cells, an effect that was also

ACCEPTED MANUSCRIPT

observed in tumors generated by MDA-shALCAM-shGal8 cells (p<0.05) at day 98 *p.i.* (Fig. 5C, left panel). Tumors generated by ALCAM-silenced cells showed significantly lower ALCAM expression (p<0.001) at day 98 *p.i.* than those generated by control or MDA-shGal8 cells at day 56 *p.i*. (Fig. 5C, right panel).

Regarding local metastasis, a tendency to reduction in the number of mice bearing metastasis in tumor-draining lymph nodes (Fig. 5D) was observed after Gal-8 and ALCAM silencing, which was not statistically significant. However, tumors generated by MDA-shGal8 cells developed only micrometastases (2/6 mice) surrounded by hyaline stroma unlike the massive metastases observed in 62.5% of the mice inoculated with control cells (Fig 5D). Remarkably, lung metastases were not observed. Thus, silencing of both Gal-8 and ALCAM synergistically slows down tumor growth in a murine model of triple negative breast cancer.

3.6 Cell surface sialylation influences MDA-MB-231 cell adhesion onto Gal-8-coated surfaces

We have previously described a predominant α(2-6) sialylation in ALCAM derived from MDA-MB-231 cells [20]. In this work, we expanded this analysis and structurally characterized the complete N-glycan profile of ALCAM by HILIC-FLR and exoglycosidase digestions (Fig. 6, Table S1). We identified 34 structures including a major proportion of complex N-glycans, with prevalent bi- or tri-antennary structures. No α(1-3,4)-antenna fucosylation was detected by specific exoglycosidase digestion, and core α(1-6)-fucosylated structures represented only 30% of the complex N-glycan structures characterized. Moreover, ALCAM complex N-glycans presented no sulfation and around 30% of sialylated structures [20]. Considering that α(2-3)-sialylated N-glycans are recognized by Gal-8 while α(2-6)-sialylated structures are not, we further analyzed sialic acid linkage type by using a specific α(2-3) neuraminidase and an α(2-3,6,8,9) neuraminidase A. Our results showed that monosialylated glycans are α(2-3)-sialylated, while the proportions of α(2-3) and α(2-6)-sialylated structures varied in di- and tri-sialylated structures. Tetrasiaylated structures were represented by approximately 2.5% of the complete profile, and, due to their low abundance, they could not be fully characterized. Interestingly, structures permissive for Gal-8 binding were detected in 45% of either α(2-3)-sialylated or neutral terminal *N*-acetyllactosamine residues (Fig. 6E). Another 18% of sialylated N-glycans could be recognized by this "*tandem-repeat*" type galectin following α(2-3,6,8,9) neuraminidase A treatment (a total of 63% of all N-glycans) (Fig. 6F). Finally, high mannose-type N-glycans (M5-M9) represented 30% of the complete profile, with Man7 being the most abundant glycan (Fig. 6, Table S1). In summary, the N-glycosylation profile of endogenous ALCAM in MDA-MB-231 cells is

ACCEPTED MANUSCRIPT

permissive for Gal-8 binding, and digestion with α(2-3,6,8,9) neuraminidase A considerably increases the number of structures recognized by this lectin.

Seeking for a correlation at the cellular level, MDA-MB-231 cells were desialylated with α(2-3,6,8,9) neuraminidase A or a specific α(2-3) neuraminidase. Sialylation before and after each treatment was assessed by flow cytometry using biotin-conjugated *Maackia amurensis* II (MAL II, a lectin capable of recognizing α(2-3) sialic acid moieties) and *Sambucus nigra* (SNA, a lectin with affinity for α(2-6)-linked sialic acid) (Fig.7A). As expected, both neuraminidases completely abrogated MAL II binding, while treatment with neuraminidase A significantly reduced SNA binding (Fig.7A). Next, cell adhesion assays were performed in 96-well tissue culture plates coated with full-length rGal-8 (5 μM; a higher lectin concentration was used in this assay to improve sensitivity of the method) or BSA as a negative control. We evaluated MDA-MB-231, MDA-shControl, MDA-shGal8, MDA-shALCAM, and MDA-shALCAM-shGal8 cells treated with α(2-3,6,8,9) neuraminidase A or α(2-3) neuraminidase. Notably, for each ALCAM$^+$ cell line (MDA-MB-231, MDA-shControl and MDA-shGal8), both neuraminidases significantly increased adhesion onto rGal-8-coated surfaces versus untreated cells or versus ALCAM-silenced cell lines (Fig. 7B). On the contrary, ALCAM-silenced cell lines only showed a tendency to increase cell adhesion after desialylation when compared to untreated cells (Fig. 7B). Thus, treatment with neuraminidases unmasks Gal-8 ligands -as reported by others [45]- and modulates Gal-8 activity, especially in ALCAM$^+$ cells. Altogether, these results showed that the combined effects of desialylated Gal-8 ligands, including ALCAM, increased MDA-MB-231 cell adhesion onto Gal-8-coated surfaces.

4. Discussion

Galectins have been proposed to serve as matricellular proteins that modulate a myriad of extracellular and intracellular events [4,6,52]. In particular, Gal-8 has been shown to act as a matrix protein capable of promoting cell adhesion by ligating and inducing clustering of several surface receptors, *i.e.* integrins, in different cell types [6,23-27]. This study reports, for the first time, that extracellular Gal-8 acts as a matrix protein promoting cell adhesion and migration via glycan-dependent ALCAM-Gal-8 interactions. ALCAM silencing in MDA-MB-231 cells decreased cell adhesion onto rGal-8-coated surfaces in a glycan-dependent manner, while in wound healing assays, ALCAM silencing decreased MDA-MB-231 cell migration both onto rGal-8-coated and uncoated culture plates. Importantly, we have shown that interaction of extracellular rGal-8 with ALCAM$^+$ cells is crucial for MDA-MB-231 cell motility, and it is glycan-dependent. On the contrary, Gal-8 silencing did not affect MDA-MB-231 cell migration

ACCEPTED MANUSCRIPT

after 20 h-treatment, which might be attributed to two events: 1) Gal-8 protein was not completely silenced in Gal-8-knocked-down cells (only 50%); 2) after 20 h-treatment, secreted Gal-8 levels were probably too low and similar between MDA-shGal8 and control cells. Therefore, we propose that extracellular Gal-8 mediates cell migration, and both cell lines secrete insufficient Gal-8 to coat plastic surfaces after 20 h-treatment. In fact, similar results were obtained by other authors as Gal-8 silencing did not affect migration after 16 h [26], whereas extracellular Gal-8 readily promoted cell motility [6,25,26]. On the other hand, the role of ALCAM in MDA-MB-231 cell migration is still under discussion: ALCAM silencing in these cells has been shown to increase cell migration on plastic and to reduce cell invasion [53], or to have no evident effect [37]. Depending on tumor type, ALCAM silencing reduced cell migration, invasion and adhesion [42], increased cell migration and invasion [38], or displayed a non-significant increase in spontaneous migration [37].

Regarding intercellular adhesion, either Gal-8 or ALCAM silencing diminished homotypic aggregation of MDA-MB-231 cells. Accordingly, silencing of Gal-8 has been shown to reduce homotypic aggregation in prostate cancer cells [54]. Moreover, and as previously shown [45], we found that exogenously-added soluble rGal-8 (1 μM) increased intercellular adhesion of Gal-8-silenced cells (data not shown). As expected, increasing concentrations of soluble rGal-8 significantly promoted enhanced cell aggregation of $ALCAM^+$ control cells, which still occurred even at high doses (5 μM, Fig. S1), highlighting the role of extracellular Gal-8 in cell-cell interactions.

Importantly, our results also showed that ALCAM is involved on cell growth, because MDA-shALCAM and MDA-shALCAM-shGal8 cells exhibited decreased cell proliferation. Likewise, ALCAM silencing reduced MDA-MB-231 cell ability to form colonies and spheroids, an effect which was likely associated to the adverse effect of ALCAM silencing on cell proliferation. Similar ALCAM effects on cell growth or colony formation have been reported by other authors in different tumor cell types [37-41,55]. Our results showed that Gal-8 silencing in MDA-MB-231 cells did not affect proliferation and colony formation, as reported for other cancer cell types [54].

Interestingly, in addition to *in vitro* effects, we also report the effects of silencing either ALCAM or Gal-8 on tumor growth in a murine model of triple negative breast cancer. Our studies indicate that dual Gal-8 and ALCAM silencing synergistically slowed down tumor growth. In agreement with our results, in xenograft murine models, Gal-8 silencing totally abolished the metastatic ability of human IGR-CaP1 prostate cancer cells when studying spontaneous metastasis to draining lymph nodes from *nude* mice, although Gal-8 did not control

ACCEPTED MANUSCRIPT

the tumorigenicity of this cell line [54]. Gal-8 overexpression transformed MDCK cells, which formed larger tumors than parental cells in immunosuppressed mice [21]. With respect to ALCAM in murine tumor models, control endometrial cancer cells inoculated into uteri developed larger tumors compared to ALCAM-silenced cells. Moreover, mice injected with ALCAM-silenced cells developed fewer local metastases than control mice [42]. Likewise, in xenograft mouse models of hepatocellular carcinoma, ALCAM knockdown induced a reduction in tumor cell growth compared to control xenografts [39,41], while ectopic expression of ALCAM demonstrated its pro-carcinogenic properties [40]. Similarly, $ALCAM^{+}$ pancreatic cancer cells were strongly tumorigenic as compared to ALCAM-silenced cells, in both subcutaneous and orthotopic mouse tumor models [38]. In metastatic models, intracardiac injection of prostate cancer cells in *nude* mice resulted in decreased bone metastasis in ALCAM-knocked down versus control cells [37].

In this study, we report the effect of MDA-MB-231 cell surface sialylation on cell adhesion onto rGal-8-coated surfaces. Noteworthy, in desialylated MDA-MB-231 cells, we observed increased adhesion to rGal-8-coated surfaces, both after removal of α(2-3,6,8,9) sialic acid residues, and after treatment with a specific α(2-3) sialidase (Fig. 7B). These results show that full length Gal-8 interactions with MDA-MB-231 cells do not completely reflect affinity data obtained with separate CRDs, as previously described for other cell types: Carlsson *et al.* [45] showed that the average binding of full-length Gal-8 to U937 monocyte cells did not significantly change after treating cells with neuraminidase A or a specific α(2-3) neuraminidase. Moreover, it has been demonstrated that treatment of predominantly α(2-3)-sialylated CHO cells with neuraminidase A increased full-length Gal-8 binding [56] and, accordingly, full-length Gal-8 binding levels to wild-type and mutant CHO cells lacking sialic acid were not significantly different [57]. Consequently, cell surface full-length Gal-8 binding to MDA-MB-231 cells also results from the combined action of both domains [45]. As affinity and avidity of lectins for glycan epitopes depend on glycan density [58], evolution has provided ways for overcoming natural heterogeneity of cell surface glycosylation and still triggering key biological events. In certain genetically-modified mice lacking specific glycosyltransferases, overall expression of glycan ligands is regulated so lectins can still bind and there are no cellular dysfunctions [59]. To summarize, in the process of Gal-8-cell binding, we propose that a higher density of *N*-acetyllactosamine (LacNAc) residues unmasked by enzymatic desialylation could compensate for the loss of α(2-3)-sialylated LacNAc.

ACCEPTED MANUSCRIPT

ALCAM N-glycosylation profiling confirmed a high percentage of permissive structures for Gal-8 recognition and binding. Evaluation of the 34 characterized structures indicated that an important proportion of glycans (45%) could be recognized by Gal-8 through interactions with either α(2-3)-sialylated or neutral terminal *N*-acetyllactosamine residues (Fig. 6E). When digested with an α(2-3,6,8,9) neuraminidase, the percentage of permissive structures considerably increased (63%) (Fig. 6F). However, as exposure of glycan epitopes is dependent on glycoconjugate structure and abundance on the cell surface, not all permissive N-glycans described for ALCAM may be exposed or recognized by Gal-8 on these cells.

To conclude, under our experimental conditions, cell desialylation increased MDA-MB-231 cell adhesion onto Gal-8-coated surfaces (Fig. 7B). The impact of cell surface desialylation cannot be only attributed to ALCAM since integrins, among others, are also Gal-8 ligands [5,6,22] present in MDA-MB-231 cells [60-62]. In this sense, Yuan *et al.* reported that desialylation of α(2-6)-sialylated integrins increased adhesive affinity between MDA-MB-231 cells and extracellular matrix proteins [60]. Accordingly, we propose that the desialylation of different Gal-8 ligands (*i.e.* ALCAM, integrins, CD44) synergistically promotes cell adhesion.

Finally, our results demonstrate that glycan-dependent heterophilic interactions between ALCAM and Gal-8 operate at the cell surface of MDA-MB-231 triple negative breast cancer cells, which contribute to modulate cell adhesion and migration. In addition, both ALCAM and Gal-8 promote tumorigenesis in a synergistic way in MDA-MB-231 cancer cells, thus cooperating in tumor progression. Overall, we propose a model in which ALCAM and Gal-8 represent not only binding partners (receptor and ligand) at the cell surface but also crucial interplaying molecules inside breast cancer cells. In fact, triple negative breast cancer represents 15-20% of all breast cancers and is characterized by a very aggressive behavior with a peak risk of recurrence within three years of diagnosis, a scenario in which effective treatments for patients are mandatory [63]. Thus, an improved understanding of the mechanisms that govern the ALCAM/Gal-8 axis may contribute to design novel therapeutic strategies, in combination with chemotherapeutic and immunotherapeutic modalities, for triple negative breast cancer patients.

5. Conclusions

In this study, we demonstrate that Gal-8 acts as a matrix protein, which promotes cell adhesion and migration through glycan-dependent interactions with ALCAM at the surface of MDA-MB-231 breast cancer cells. Importantly, we found that cell sialylation modulates Gal-8-mediated cell adhesion. Notably, either Gal-8 or ALCAM silencing diminishes cell-cell

ACCEPTED MANUSCRIPT

aggregation, thus emphasizing the influence of both molecules in tumorigenesis. In addition, ALCAM silencing reduced MDA-MB-231 cell ability to proliferate, influencing colony and spheroid formation. Interestingly, in a triple negative breast cancer model, ALCAM and Gal-8 acted synergistically to promote tumorigenesis. Of note, this is the first evidence demonstrating the effect of dual ALCAM and Gal-8 silencing on tumor growth in triple negative breast cancer. Further elucidation of the mechanisms through which the ALCAM/Gal-8 axis fuels tumorigenesis may contribute to design new drugs for triple negative breast cancer therapy.

Acknowledgements

F.F. is a fellow from Consejo Nacional de Investigaciones Científicas y Técnicas (CONICET). M.T.E, K.V.M., G.A.R, A.J.C., L.L.C and M.F.T. are researchers from CONICET.

Funding

This work was supported by Agencia Nacional de Promoción Científica y Tecnológica [PICT-2007-1631 and PICT-2012-0071 to MTE; PICT-2015-0564 to KVM], and CONICET [PIP-2015-1122015-0100647 to MFT]. GAR, KVM and AJC acknowledge support from Fundación Sales, Fundación René Barón and Fundación Bunge & Born.

Authors' contributions

MTE, LLC, GAR and KVM: conceived and designed experiments; analyzed and interpreted data; wrote and revised the manuscript. FF, AJC, LLC and CST: executed experiments, analyzed data, and revised the manuscript. SIV: performed histopathological studies, analyzed and interpreted data. MFT and CWT: analyzed and interpreted data, and revised the manuscript.

Disclosure of Potential Conflicts of Interest

The authors declare no competing financial interests.

Abbreviations

A, absorbance; 2AB, 2-aminobenzamide; ALCAM, activated leukocyte cell adhesion molecule; Bcl-2, B-cell lymphoma 2 protein; BSA, bovine serum albumin; CRD, carbohydrate recognition domain; DABCO, diazabicyclo[2.2.2]octane; DAPI, 4',6-diamidino-2-phenylindole; DMEM, Dulbecco's Modified Eagle Medium; EDTA, ethylene-diaminetetraacetic acid; FBS, fetal bovine serum; FLR, Fluorescence detector; Gal-8, galectin-8; HILIC, Hydrophilic interaction liquid chromatography; HRP, horseradish peroxidase; MAL II, *Maackia amurensis* II lectin;

ACCEPTED MANUSCRIPT

MTT, 3-[4,5-dimethylthiazol-2-yl]-2,5-diphenyltetrazolium bromide; PBS, phosphate-buffered saline; PE, phycoerythrin; PMSF, phenylmethylsulfonyl fluoride; PVDF, polyvinylidene-difluoride; rGal-8, recombinant galectin-8; SDS-PAGE, sodium dodecyl sulphate-polyacrylamide gel electrophoresis; shRNA, short hairpin RNA; shGal-8, shRNA specific for galectin-8; shALCAM, shRNA specific for ALCAM; SNA, *Sambucus nigra* agglutinin; SPR, surface plasmon resonance; WAX, Weak Anion Exchange chromatography.

References

[1] J.P. Cerliani, A.G. Blidner, M.A. Toscano, D.O. Croci, G.A. Rabinovich, Translating the 'sugar code' into immune and vascular signaling programs, Trends Biochem. Sci. 42 (2017) 255-273.

[2] M.T. Elola, F. Ferragut, S.P. Méndez-Huergo, D.O. Croci, C. Bracalente, G.A. Rabinovich, Galectins: Multitask signaling molecules linking fibroblast, endothelial and immune cell programs in the tumor microenvironment, Cell. Immunol. 333 (2018) 34-45.

[3] N. Bidon, F. Brichory, S. Hanash, P. Bourguet, L. Dazord, J.P. Le Pennec, Two messenger RNAs and five isoforms for Po66-CBP, a galectin-8 homolog in a human lung carcinoma cell line, Gene 274 (2001) 253-262.

[4] Y. Zick, M. Eisenstein, R.A. Goren, Y.R. Hadari, Y. Levy, D. Ronen, Role of galectin-8 as a modulator of cell adhesion and cell growth, Glycoconj. J. 19 (2004) 517-526.

[5] Y.R. Hadari, R. Arbel-Goren, Y. Levy, A. Amsterdam, R. Alon, R. Zakut, Y. Zick, Galectin-8 binding to integrins inhibits cell adhesion and induces apoptosis, J. Cell Sci. 113 (2000) 2385-2397.

[6] Y. Levy, R. Arbel-Goren, Y.R. Hadari, S. Eshhar, D. Ronen, E. Elhanany, B. Geiger, Y. Zick, Galectin-8 functions as a matricellular modulator of cell adhesion, J. Biol. Chem. 276 (2001) 31285-31295.

[7] Y. Levy, D. Ronen, A.D. Bershadsky, Y. Zick, Sustained induction of ERK, protein kinase B, and p70 S6 kinase regulates cell spreading and formation of F-actin microspikes upon ligation of integrins by galectin-8, a mammalian lectin, J. Biol. Chem. 278 (2003) 14533-14542.

[8] R. Arbel-Goren, Y. Levy, D. Ronen, Y. Zick, Cyclin-dependent kinase inhibitors and JNK act as molecular switches, regulating the choice between growth arrest and apoptosis induced by galectin-8, J. Biol. Chem. 280 (2005) 19105-19114.

ACCEPTED MANUSCRIPT

[9] S.R. Stowell, C.M. Arthur, M. Dias-Baruffi, L.C. Rodrigues, J.P. Gourdine, J. Heimburg-Molinaro, T. Ju, R.J. Molinaro, C. Rivera-Marrero, B. Xia, D.F. Smith, R.D. Cummings, Innate immune lectins kill bacteria expressing blood group antigen, Nat. Med. 16 (2010) 295-301.

[10] T.L. Thurston, M.P. Wandel, N. von Muhlinen, A. Foeglein, F. Randow, Galectin 8 targets damaged vesicles for autophagy to defend cells against bacterial invasion, Nature 482 (2012) 414-418.

[11] B. Falcon, J. Noad, H. McMahon, F. Randow, M. Goedert, Galectin-8-mediated selective autophagy protects against seeded tau aggregation, J. Biol. Chem. 293 (2018) 2438-2451.

[12] J.F. Sampson, A. Suryawanshi, W.S. Chen, G.A. Rabinovich, N. Panjwani, Galectin-8 promotes regulatory T-cell differentiation by modulating IL-2 and TGFbeta signaling, Immunol. Cell Biol. 94 (2016) 213-219.

[13] A. Danguy, S. Rorive, C. Decaestecker, Y. Bronckart, H. Kaltner, Y.R. Hadari, R. Goren, Y. Zich, M. Petein, I. Salmon, H.J. Gabius, R. Kiss, Immunohistochemical profile of galectin-8 expression in benign and malignant tumors of epithelial, mesenchymatous and adipous origins, and of the nervous system, Histol. Histopathol. 16 (2001) 861-868.

[14] H. Lahm, S. Andre, A. Hoeflich, J.R. Fischer, B. Sordat, H. Kaltner, E. Wolf, H.J. Gabius, Comprehensive galectin fingerprinting in a panel of 61 human tumor cell lines by RT-PCR and its implications for diagnostic and therapeutic procedures, J. Cancer Res. Clin. Oncol. 127 (2001) 375-386.

[15] N. Bidon-Wagner, J.P. Le Pennec, Human galectin-8 isoforms and cancer, Glycoconj. J. 19 (2004) 557-563.

[16] M.T. Elola, F. Ferragut, V.M. Cardenas Delgado, L.G. Nugnes, L. Gentilini, D. Laderach, M.F. Troncoso, D. Compagno, C. Wolfenstein-Todel, G.A. Rabinovich, Expression, localization and function of galectin-8, a tandem-repeat lectin, in human tumors, Histol. Histopathol. 29 (2014) 1093-1105.

[17] Y. Vinik, H. Shatz-Azoulay, Y. Zick, Molecular mechanisms underlying the role of galectin-8 as a regulator of cancer growth and metastasis, Trends Glycosci. Glyc. 30 (2018) SE119-SE128.

[18] H. Lu, K.L. Knutson, E. Gad, M.L. Disis, The tumor antigen repertoire identified in tumor-bearing neu transgenic mice predicts human tumor antigens, Cancer Res. 66 (2006) 9754-9761.

[19] H. Barrow, X. Guo, H.H. Wandall, J.W. Pedersen, B. Fu, Q. Zhao, C. Chen, J.M. Rhodes, L.G. Yu, Serum galectin-2, -4, and -8 are greatly increased in colon and breast

ACCEPTED MANUSCRIPT

cancer patients and promote cancer cell adhesion to blood vascular endothelium, Clin. Cancer Res. 17 (2011) 7035-7046.

[20] M.M. Fernández, F. Ferragut, V.M. Cardenas Delgado, C. Bracalente, A.I. Bravo, A.J. Cagnoni, M. Nunez, L.G. Morosi, H.R. Quinta, M.V. Espelt, M.F. Troncoso, C. Wolfenstein-Todel, K.V. Marino, E.L. Malchiodi, G.A. Rabinovich, M.T. Elola, Glycosylation-dependent binding of galectin-8 to activated leukocyte cell adhesion molecule (ALCAM/CD166) promotes its surface segregation on breast cancer cells, Biochim. Biophys. Acta 1860 (2016) 2255-2268.

[21] C. Oyanadel, C. Holmes, E. Pardo, C. Retamal, R. Shaughnessy, P. Smith, P. Cortes, M. Bravo-Zehnder, C. Metz, T. Feuerhake, D. Romero, J.C. Roa, V. Montecinos, A. Soza, A. Gonzalez, Galectin-8 induces partial epithelial-mesenchymal transition with invasive tumorigenic capabilities involving a FAK/EGFR/proteasome pathway in Madin-Darby canine kidney cells, Mol. Biol. Cell 29 (2018) 557-574.

[22] C. Cárcamo, E. Pardo, C. Oyanadel, M. Bravo-Zehnder, P. Bull, M. Cáceres, J. Martínez, L. Massardo, S. Jacobelli, A. González, A. Soza, Galectin-8 binds specific beta1 integrins and induces polarized spreading highlighted by asymmetric lamellipodia in Jurkat T cells, Exp. Cell Res. 312 (2006) 374-386.

[23] Y. Levy, S. Auslender, M. Eisenstein, R.R. Vidavski, D. Ronen, A.D. Bershadsky, Y. Zick, It depends on the hinge: a structure-functional analysis of galectin-8, a tandem-repeat type lectin, Glycobiology 16 (2006) 463-476.

[24] S. Diskin, W.S. Chen, Z. Cao, S. Gyawali, H. Gong, A. Soza, A. Gonzalez, N. Panjwani, Galectin-8 promotes cytoskeletal rearrangement in trabecular meshwork cells through activation of Rho signaling, PLoS One 7 (2012) e44400.

[25] I. Camby, N. Belot, S. Rorive, F. Lefranc, C.A. Maurage, H. Lahm, H. Kaltner, Y. Hadari, M.M. Ruchoux, J. Brotchi, Y. Zick, I. Salmon, H.J. Gabius, R. Kiss, Galectins are differentially expressed in supratentorial pilocytic astrocytomas, astrocytomas, anaplastic astrocytomas and glioblastomas, and significantly modulate tumor astrocyte migration, Brain Pathol. 11 (2001) 12-26.

[26] C. Metz, R. Doger, E. Riquelme, P. Cortes, C. Holmes, R. Shaughnessy, C. Oyanadel, C. Grabowski, A. Gonzalez, A. Soza, Galectin-8 promotes migration and proliferation and prevents apoptosis in U87 glioblastoma cells, Biol. Res. 49 (2016) 33.

[27] N.E. Reticker-Flynn, D.F. Malta, M.M. Winslow, J.M. Lamar, M.J. Xu, G.H. Underhill, R.O. Hynes, T.E. Jacks, S.N. Bhatia, A combinatorial extracellular matrix platform

ACCEPTED MANUSCRIPT

identifies cell-extracellular matrix interactions that correlate with metastasis, Nat. Commun. 3 (2012) 1122.

[28] L.N. Cueni, M. Detmar, Galectin-8 interacts with podoplanin and modulates lymphatic endothelial cell functions, Exp. Cell Res. 315 (2009) 1715-1723.

[29] V.M. Delgado, L.G. Nugnes, L.L. Colombo, M.F. Troncoso, M.M. Fernandez, E.L. Malchiodi, I. Frahm, D.O. Croci, D. Compagno, G.A. Rabinovich, C. Wolfenstein-Todel, M.T. Elola, Modulation of endothelial cell migration and angiogenesis: a novel function for the "tandem-repeat" lectin galectin-8, FASEB J. 25 (2011) 242-254.

[30] M. Friedel, S. Andre, H. Goldschmidt, H.J. Gabius, R. Schwartz-Albiez, Galectin-8 enhances adhesion of multiple myeloma cells to vascular endothelium and is an adverse prognostic factor, Glycobiology 26 (2016) 1048-1058.

[31] J. Etulain, S. Negrotto, M.V. Tribulatti, D.O. Croci, J. Carabelli, O. Campetella, G.A. Rabinovich, M. Schattner, Control of angiogenesis by galectins involves the release of platelet-derived proangiogenic factors., PLoS One 9 (2014) e96402.

[32] Y. Vinik, H. Shatz-Azoulay, A. Vivanti, N. Hever, Y. Levy, R. Karmona, V. Brumfeld, S. Baraghithy, M. Attar-Lamdar, S. Boura-Halfon, I. Bab, Y. Zick, The mammalian lectin galectin-8 induces RANKL expression, osteoclastogenesis, and bone mass reduction in mice, Elife 4 (2015) e05914.

[33] Y. Vinik, H. Shatz-Azoulay, S. Hiram-Bab, L. Kandel, Y. Gabet, G. Rivkin, Y. Zick, Ablation of the mammalian lectin galectin-8 induces bone defects in mice, FASEB J. 32 (2018) 2366-2380.

[34] G.W. Swart, P.C. Lunter, J.W. Kilsdonk, L.C. Kempen, Activated leukocyte cell adhesion molecule (ALCAM/CD166): signaling at the divide of melanoma cell clustering and cell migration?, Cancer Metastasis Rev. 24 (2005) 223-236.

[35] A.G. Hansen, G.W. Swart, A. Zijlstra, ALCAM: basis sequence: mouse, AFCS Nat. Mol. Pages 2011 (2011).

[36] K.E. Hebron, E.Y. Li, S.A. Arnold Egloff, A.K. von Lersner, C. Taylor, J. Houkes, D.K. Flaherty, A. Eskaros, T.P. Stricker, A. Zijlstra, Alternative splicing of ALCAM enables tunable regulation of cell-cell adhesion through differential proteolysis., Sci. Rep. 8 (2018) 3208.

[37] A.G. Hansen, S.A. Arnold, M. Jiang, T.D. Palmer, T. Ketova, A. Merkel, M. Pickup, S. Samaras, Y. Shyr, H.L. Moses, S.W. Hayward, J.A. Sterling, A. Zijlstra, ALCAM/CD166 is a TGF-beta-responsive marker and functional regulator of prostate cancer metastasis to bone, Cancer Res. 74 (2014) 1404-1415.

ACCEPTED MANUSCRIPT

[38] K. Fujiwara, K. Ohuchida, M. Sada, K. Horioka, C.D. Ulrich, K. Shindo, T. Ohtsuka, S. Takahata, K. Mizumoto, Y. Oda, M. Tanaka, CD166/ALCAM expression is characteristic of tumorigenicity and invasive and migratory activities of pancreatic cancer cells, PLoS One 9 (2014) e107247.

[39] L. Ma, J. Wang, J. Lin, Q. Pan, Y. Yu, F. Sun, Cluster of differentiation 166 (CD166) regulated by phosphatidylinositide 3-Kinase (PI3K)/AKT signaling to exert its anti-apoptotic role via yes-associated protein (YAP) in liver cancer, J. Biol. Chem. 289 (2014) 6921-6933.

[40] W. Yu, J. Wang, L. Ma, X. Tang, Y. Qiao, Q. Pan, Y. Yu, F. Sun, CD166 plays a pro-carcinogenic role in liver cancer cells via inhibition of FOXO proteins through AKT, Oncol. Rep. 32 (2014) 677-683.

[41] X. Tang, X. Chen, Y. Xu, Y. Qiao, X. Zhang, Y. Wang, Y. Guan, F. Sun, J. Wang, CD166 positively regulates MCAM via inhibition to ubiquitin E3 ligases Smurf1 and betaTrCP through PI3K/AKT and c-Raf/MEK/ERK signaling in Bel-7402 hepatocellular carcinoma cells, Cell. Signal. 27 (2015) 1694-1702.

[42] L. Devis, C.P. Moiola, N. Masia, E. Martinez-Garcia, M. Santacana, T.V. Stirbat, F. Brochard-Wyart, A. Garcia, F. Alameda, S. Cabrera, J. Palacios, G. Moreno-Bueno, M. Abal, W. Thomas, S. Dufour, X. Matias-Guiu, A. Santamaria, J. Reventos, A. Gil-Moreno, E. Colas, Activated leukocyte cell adhesion molecule (ALCAM) is a marker of recurrence and promotes cell migration, invasion, and metastasis in early-stage endometrioid endometrial cancer, J. Pathol. 241 (2017) 475-487.

[43] J. Hirabayashi, T. Hashidate, Y. Arata, N. Nishi, T. Nakamura, M. Hirashima, T. Urashima, T. Oka, M. Futai, W.E. Muller, F. Yagi, K. Kasai, Oligosaccharide specificity of galectins: a search by frontal affinity chromatography, Biochim. Biophys. Acta 1572 (2002) 232-254.

[44] H. Ideo, A. Seko, I. Ishizuka, K. Yamashita, The N-terminal carbohydrate recognition domain of galectin-8 recognizes specific glycosphingolipids with high affinity, Glycobiology 13 (2003) 713-723.

[45] S. Carlsson, C.T. Oberg, M.C. Carlsson, A. Sundin, U.J. Nilsson, D. Smith, R.D. Cummings, J. Almkvist, A. Karlsson, H. Leffler, Affinity of galectin-8 and its carbohydrate recognition domains for ligands in solution and at the cell surface, Glycobiology 17 (2007) 663-676.

ACCEPTED MANUSCRIPT

[46] H. Ideo, T. Matsuzaka, T. Nonaka, A. Seko, K. Yamashita, Galectin-8-N-domain recognition mechanism for sialylated and sulfated glycans, J. Biol. Chem. 286 (2011) 11346-11355.

[47] H. Yoshida, S. Yamashita, M. Teraoka, A. Itoh, S. Nakakita, N. Nishi, S. Kamitori, X-ray structure of a protease-resistant mutant form of human galectin-8 with two carbohydrate recognition domains, FEBS J. 279 (2012) 3937-3951.

[48] P.H. Jensen, N.G. Karlsson, D. Kolarich, N.H. Packer, Structural analysis of N- and O-glycans released from glycoproteins, Nat. Protoc. 7 (2012) 1299-1310.

[49] L. Royle, R.A. Dwek, P.M. Rudd, Determining the structure of oligosaccharides N- and O-linked to glycoproteins, in Curr. Protoc. Protein Sci., 2006, pp. 1-45.

[50] R. Saldova, A. Asadi Shehni, V.D. Haakensen, I. Steinfeld, M. Hilliard, I. Kifer, A. Helland, Z. Yakhini, A.L. Børresen-Dale, P.M. Rudd, Association of N-Glycosylation with breast carcinoma and systemic features using High-Resolution Quantitative UPLC, J. Proteome Res. 13 (2014) 2314-2327.

[51] K. Mariño, J. Bones, J.J. Kattla, P.M. Rudd, A systematic approach to protein glycosylation analysis: a path through the maze, Nat. Chem. Biol. 6 (2010) 713-723.

[52] M.T. Elola, C. Wolfenstein-Todel, M.F. Troncoso, G.R. Vasta, G.A. Rabinovich, Galectins: matricellular glycan-binding proteins linking cell adhesion, migration, and survival, Cell Mol. Life Sci. 64 (2007) 1679-1700.

[53] S. Hein, V. Muller, N. Kohler, H. Wikman, S. Krenkel, T. Streichert, M. Schweizer, S. Riethdorf, V. Assmann, M. Ihnen, K. Beck, R. Issa, F. Janicke, K. Pantel, K. Milde-Langosch, Biologic role of activated leukocyte cell adhesion molecule overexpression in breast cancer cell lines and clinical tumor tissue, Breast Cancer Res. Treat. 129 (2011) 347-360.

[54] L.D. Gentilini, F.M. Jaworski, C. Tiraboschi, I.G. Perez, M.L. Kotler, A. Chauchereau, D.J. Laderach, D. Compagno, Stable and high expression of Galectin-8 tightly controls metastatic progression of prostate cancer, Oncotarget 8 (2017) 44654-44668.

[55] A. Jezierska, W. Matysiak, T. Motyl, ALCAM/CD166 protects breast cancer cells against apoptosis and autophagy, Med. Sci. Monit. 12 (2006) BR263-273.

[56] A.K. Ludwig, M. Michalak, N. Shilova, S. Andre, H. Kaltner, N.V. Bovin, J. Kopitz, H.J. Gabius, Studying the structural significance of galectin design by playing a modular puzzle: homodimer generation from human tandem-repeat-type (heterodimeric) galectin-8 by domain shuffling, Molecules 22 (2017) 1572.

ACCEPTED MANUSCRIPT

[57] S.K. Patnaik, B. Potvin, S. Carlsson, D. Sturm, H. Leffler, P. Stanley, Complex N-glycans are the major ligands for galectin-1, -3, and -8 on Chinese hamster ovary cells, Glycobiology 16 (2006) 305-317.

[58] T.K. Dam, F.C. Brewer, Maintenance of cell surface glycan density by lectin-glycan interactions: A homeostatic and innate immune regulatory mechanism, Glycobiology 20 (2010) 1061-1064.

[59] J.W. Dennis, C.F. Brewer, Density-dependent lectin-glycan interactions as a paradigm for conditional regulation by posttranslational modifications, Moll. Cell. Proteomics 12 (2013) 913-920.

[60] Y. Yuan, L. Wu, S. Shen, S. Wu, M.M. Burdick, Effect of alpha 2,6 sialylation on integrin-mediated adhesion of breast cancer cells to fibronectin and collagen IV, Life Sci. 149 (2016) 138-145.

[61] J. Lu, T. Isaji, S. Im, T. Fukuda, A. Kameyama, J. Gu, Expression of N-acetylglucosaminyltransferase III suppresses α2,3-sialylation, and its distinctive functions in cell migration are attributed to α2,6-sialylation levels, J. Biol. Chem. 291 (2016) 5708-5720.

[62] T. Isaji, S. Im, A. Kameyama, Y. Wang, T. Fukuda, J. Gu, A complex between phosphatidylinositol 4 kinase IIα and integrin α3β1 is required for N-glycan sialylation in cancer cells, J. Biol. Chem. (2019) doi: 10.1074/jbc.RA1118.005208.

[63] J.M. Lebert, R. Lester, E. Powell, M. Seal, J. McCarthy, Advances in the systemic treatment of triple-negative breast cancer, Curr. Oncol. 25 (2018) S142-S150.

[64] A. Varki, R.D. Cummings, M. Aebi, N.H. Packer, P.H. Seeberger, J.D. Esko, P. Stanley, G. Hart, A. Darvill, T. Kinoshita, J.J. Prestegard, R.L. Schnaar, H.H. Freeze, J.D. Marth, C.R. Bertozzi, M.E. Etzler, M. Frank, J.F.G. Vliegenthart, T. Lütteke, S. Perez, E. Bolton, P. Rudd, J. Paulson, M. Kanehisa, P. Toukach, K.F. Aoki-Kinoshita, A. Dell, H. Narimatsu, W. York, N. Taniguchi, S. Kornfeld, Symbol nomenclature for graphical representations of glycans, Glycobiology 25 (2015) 1323-1324.

ACCEPTED MANUSCRIPT

Figure legends

Figure 1. Silencing ALCAM in MDA-MB-231 breast cancer cells decreases cell adhesion onto Gal-8-coated surfaces in a glycan-dependent manner. Western blot analysis of Gal-8 (A, upper panel) and ALCAM (B, upper panel) expression in whole lysates from MDA-MB-231, mock-transduced MDA-MB-231 (MDA-shControl), MDA-MB-231-shALCAM (MDA-shALCAM), MDA-MB-231-shGal-8 (MDA-shGal8), and MDA-MB-231-shALCAM-shGal-8 (MDA-shALCAM-shGal8) cells. Lysates were run in parallel in the same 10% gel in SDS-PAGE, and then transferred onto PVDF membranes. Blots were probed with primary antibodies, followed by the incubation with the appropriate secondary antibody conjugated to HRP and detection by chemiluminiscence. The bar graphs show Gal-8 (A, lower panel) and ALCAM (B, lower panel) protein expression in densitometric analysis; β-actin was used to normalize protein loading. Data were analyzed by one-way ANOVA with Tukey post-test (n=7). Asterisks (***) denote a statistically significant difference with $p<0.001$. (C) Dose-response curves of cell adhesion assays onto full-length rGal-8 (0.25-3 μM) or BSA as substrates, obtained by incubating MDA-MB-231, MDA-shControl, MDA-shGal8, MDA-shALCAM, and MDA-shALCAM-shGal8 cells (2×10^4 cells/well) during 1 h. A: absorbance at 595 nm. Data were analyzed by two-way ANOVA with Tukey post-test (n=5). *$p<0.05$. (D) Indirect immunofluorescence staining for cell surface expression of endogenous ALCAM in non-permeabilized MDA-MB-231, MDA-shControl, MDA-shALCAM and MDA-shALCAM-shGal8 cells, as evaluated by confocal microscopy. Endogenous ALCAM was developed with an unconjugated anti-ALCAM monoclonal antibody followed by an Alexa 555-conjugated secondary antibody (red, left panel). Merged images of DAPI staining (nuclei, blue) and phase contrast are also shown (right panel). Each experiment was performed three times with reproducible results. Scale bars: 10 μm. (E) Cell adhesion assays onto full-length rGal-8 (2 μM) as a substrate were performed by incubating MDA-MB-231, MDA-shControl, MDA-shGal8, MDA-shALCAM, and MDA-shALCAM-shGal8 cells (2×10^4 cells/well) during 1 h in the presence of lactose (100 mM), a disaccharide which binds to Gal-8 CRDs, or the unrelated disaccharide sucrose (100 mM). A: absorbance at 595 nm. Data were analyzed by two-way ANOVA with Bonferroni post-test (n=4). *$p<0.05$. Values in Fig. 1 A,B,C,E are presented as mean values ± S.E.M. with differences at $p\leq0.05$ considered as significant. n.s.: differences were not statistically significant.

ACCEPTED MANUSCRIPT

Figure 2. Silencing ALCAM in MDA-MB-231 breast cancer cells decreases cell migration onto Gal-8-coated surfaces in a glycan-dependent fashion. (A) Wound healing assays were performed as described in *Materials and Methods*, onto surfaces without or with full-length rGal-8 (2 μM) coating. To evaluate wound closure, MDA-MB-231, MDA-shControl, MDA-shGal8, MDA-shALCAM, and MDA-shALCAM-shGal8 cells were incubated with DMEM without FBS for 20 h at 37 ºC. *Image J* software was used to determine the whole area of the wound at each incubation time. Values represent the mean ± S.E.M. of the percentage of wound closure at 20 h versus 0 h. Data were analyzed by two-way ANOVA with Bonferroni post-test (n=7). ***p<0.001; **p<0.01. (B) Cell migration onto surfaces without (left panel) or with full-length rGal-8 (2 μM) coating (right panel) was determined by wound closure and photographed at 0 and 20 h for MDA-MB-231, MDA-shControl, MDA-shGal8, MDA-shALCAM, and MDA-shALCAM-shGal8 cells. Representative photographs are shown. Scale bars: 0.1 mm. (C) Cell migration onto full-length rGal-8 (2 μM) as a substrate was quantified in the presence of 100 mM lactose or 100 mM sucrose. Values represent the mean ± S.E.M., and data were analyzed by two-way ANOVA with Bonferroni post-test (n=7). ***p<0.001; **p<0.01; *p<0.05. (D) Effects of lactose (100 mM; left panel) and sucrose (100 mM; right panel) on cell migration onto immobilized rGal-8 are shown in representative photographs. Scale bars: 0.1 mm. n.s.: differences were not statistically significant.

Figure 3. Silencing of Gal-8 or ALCAM in MDA-MB-231 breast cancer cells decreases cell-cell adhesion. (A) MDA-MB-231, MDA-shControl, MDA-shGal8, MDA-shALCAM, and MDA-shALCAM-shGal8 single-cell suspensions were incubated in FBS-free DMEM with gentle rotation at 37 °C for 1 h. Each sample was loaded onto different wells of 96-well plates to be photographed, and the number of free cells was counted at 0 and 1 h in five fields per sample. Aggregation was calculated as the percentages of free cells incubated in the absence of exogenous rGal-8. Each assay was performed in triplicates, and values represent the mean ± S.E.M. Data were analyzed by one-way ANOVA with Tukey post-test (n=4). *p<0.05. (B) Representative photographs of MDA-MB-231, MDA-shControl, MDA-shGal8, MDA-shALCAM, and MDA-shALCAM-shGal8 cell aggregation performed without adding exogenous rGal-8. Each inset represents a magnification of the corresponding photograph. n.s.: differences were not statistically significant.

ACCEPTED MANUSCRIPT

Figure 4. ALCAM silencing inhibits cell proliferation in MDA-MB-231 breast cancer cells. (A) MDA-MB-231, MDA-shControl, MDA-shGal8, MDA-shALCAM, and MDA-shALCAM-shGal8 cell proliferation was evaluated in MTT assays. Formazan crystals formed in viable cells were dissolved in dimethyl sulfoxide, and absorbance was measured at 595 nm. Cell proliferation was measured after 0, 24, 48, 72 and 96 h as described in *Materials and Methods*. At 96 h, both MDA-shALCAM ($p<0.05$; $p<0.01$) and MDA-shALCAM-shGal8 ($p<0.001$; $p<0.001$) cells showed decreased proliferation compared to control MDA-MB-231 and MDA-shControl cells, respectively. MDA-shALCAM ($p<0.01$) and MDA-shALCAM-shGal8 ($p<0.001$) cells also showed decreased proliferation compared to MDA-shGal8 cells. Data were analyzed by two-way ANOVA with Holm-Sídák post-test (n=6). ***$p<0.001$; **$p<0.01$; *$p<0.05$. (B) Colony formation ability of single cells was evaluated. Cells were incubated for 10 days at 37 °C. Finally, cells were fixed in paraformaldehyde and stained with crystal violet, and colonies were photographed and quantified. Data were analyzed by one-way ANOVA with Tukey post-test (n=7). ***$p<0.001$. (C) Spheroid-formation assay was performed by seeding MDA-MB-231, MDA-shControl, MDA-shGal8, MDA-shALCAM, and MDA-shALCAM-shGal8 cells onto matrigel. Spheroids were photographed after 3, 7 and 10 days of incubation (left panel). Spheroid volumes versus the incubation time were also plotted (right panel). Data were analyzed by two-way ANOVA with Bonferroni post-test (n=3). ***$p<0.001$; **$p<0.01$. Scale bars (3, 7, 10 days): 50 μm. Values in Fig. 4 A-C are presented as mean ± S.E.M. n.s.: differences were not statistically significant.

Figure 5. Dual targeting of ALCAM and Gal-8 decreases primary tumor size in a murine model of triple negative breast cancer. (A) MDA-MB-231, MDA-shControl, MDA-shGal8, MDA-shALCAM, and MDA-shALCAM-shGal8 human breast cancer cells were subcutaneously inoculated in *nude* mice in the presence of matrigel. Tumor volume was evaluated 2-3 times a week. Gal-8 and ALCAM silencing significantly delayed the growth of primary tumors. Control mice were euthanized because of ethical reasons at day 56 *post-inoculum* as well as mice inoculated with MDA-shGal8 cells for comparison. Mice injected with MDA-shALCAM and MDA-shALCAM-shGal8 cells (which tumors were considerably small at day 56 *post-inoculum*) were kept alive until 98 days *post-inoculum*. At day 98, tumors generated by MDA-shALCAM-shGal8 cells proved to be smaller than those generated by MDA-shALCAM cells. **$p<0.01$; *$p<0.05$. Values represent the mean ± S.E.M. from two independent experiments, and were analyzed by Chi-square test. (B) Photographs of representative primary tumors derived from MDA-MB-231, MDA-shControl, MDA-shGal8, MDA-shALCAM, and MDA-shALCAM-

ACCEPTED MANUSCRIPT

shGal8 cells were taken at 56 days *post-inoculum*. Scale bars: 1 cm. (C) Western blot experiments showing significantly decreased Gal-8 protein levels at day 56 *post-inoculum* ($p<0.01$) in tumors derived from MDA-shGal8 cells as compared to those generated by control cells, an effect that was also statistically significant in tumors derived from MDA-shALCAM-shGal8 cells at day 98 *post-inoculum* as compared to those generated by control cells ($p<0.05$) (left panel). ALCAM expression levels were significantly reduced ($p<0.001$) in tumors generated by ALCAM-silenced (MDA-shALCAM and MDA-shALCAM-shGal8) cells at day 98 as compared to those generated by control and MDA-shGal8 cells at day 56 (right panel). Values represent the mean ± S.E.M., and data were analyzed by one-way ANOVA with Bonferroni post-test (n=4). ***$p<0.001$; **$p<0.01$; *$p<0.05$. (D) Representative photographs of haematoxylin and eosin staining performed in tumor-draining lymph node sections. A lymph node section without metastasis (left panel) from mice inoculated with control MDA-MB-231 cells is shown (magnification: x5). A lymph node with metastasis (central panel) from mice inoculated with control MDA-MB-231 cells is shown (magnification: x5). The two insets (magnification: x40) display metastatic foci (a), and lymphatic vessel invasion by tumor cells (b). Lymph node with micrometastasis (right panel) derived from inoculated MDA-shGal8 cells is shown (magnification: x5; inset magnification: x40). Scale bars: 500 µm. n.s.: differences were not statistically significant.

Figure 6. N-glycosylation profile of ALCAM purified from MDA-MB-231 cells. (A) N-Glycan analysis by hydrophilic interaction liquid chromatography (HILIC). Released N-glycans were labeled with 2AB, and the scale of glucose units (GU) is based on the elution of the 2AB labeled glucose ladder. Glycans were represented according to the symbol nomenclature proposed by [64]. Only the major species have been shown (a detailed N-glycan structural characterization is presented in supplemental Table S1). N-glycans are coloured according to their structure, *i.e.* red for neutral (N), blue for monosialylated (S1), green for disialylated (S2), purple for trisialylated (S3) and orange for tetrasialylated (S4) structures. (B) Relative abundance of the different N-glycan groups (neutral, mono-, di-, tri- and tetra-sialylated) described in (A). ALCAM N-glycoprofiling shows high abundance of non-sialylated glycans and relatively high proportions of di- and trisialylated glycans. (C) Relative abundance of high mannose (HM) and complex N-glycans. Complex glycans are divided based on their antennarity (A1, monoantennary; A2, biantennary; A3 triantennary and A4, tetraantennary), showing mostly complex N-glycans with major proportions of di- and triantennary structures. (D) Sialic acid linkage in complex N-glycans. Analysis, comparing sialylated antennae in different glycan species, showed a higher

ACCEPTED MANUSCRIPT

proportion of α(2-6) sialylation. (E) Relative abundance of MDA-MB-231 endogenous ALCAM N-glycans permissive and non-permissive for Gal-8 binding. (F) Relative abundance of MDA-MB-231 endogenous ALCAM N-glycans permissive and non-permissive for Gal-8 binding, after treatment with α(2-3,6,8,9) neuraminidase A.

Figure 7. Cell surface sialylation influences MDA-MB-231 breast cancer cell interaction with immobilized Gal-8 and compromise cell adhesion. (A) Flow cytometry analysis of the glycophenotype of MDA-MB-231 cells treated with α(2-3,6,8,9) neuraminidase A (green), α(2-3) neuraminidase (blue) or without any glycosidase (grey), detected with biotinylated plant lectins (MAL II or SNA) followed by phycoerythrin-conjugated streptavidin. Negative controls were performed by treating cells with phycoerythrin-conjugated streptavidin alone, without any plant lectin (red). PE: phycoerythrin. Normalized number of events plotted: 10,000. (B) Cell adhesion assays were performed in 96-well tissue culture plates coated with full-length rGal-8 (5 μM, to improve method sensitivity) or BSA. MDA-MB-231, MDA-shControl, MDA-shGal8, MDA-shALCAM, and MDA-shALCAM-shGal8 cells (3×10^4 cells/well) were treated with α(2-3,6,8,9) neuraminidase A (green) and α(2-3) neuraminidase (blue) and compared with each untreated cell line (grey), after incubating for 2 h onto rGal-8-coated surfaces. Neuraminidase A treatment increased cell adhesion onto rGal-8 as compared to untreated cells for each $ALCAM^+$ cell line (MDA-MB-231: $p<0.01$; MDA-shControl: $p<0.01$; MDA-shGal8: $p<0.05$). Treatment with α(2-3) neuraminidase also increased cell adhesion onto rGal-8 in MDA-MB-231, MDA-shControl and MDA-shGal8cells ($p<0.05$) as compared to each untreated cell line. Each treatment for $ALCAM^+$ cell lines increased cell adhesion ($p<0.001$) onto rGal-8 as compared to the same treatment in ALCAM-silenced cell lines. A: Absorbance at 595 nm. Data in Fig. 7 B are presented as mean values ± S.E.M., and were analyzed by two-way ANOVA with Sídák post-test (n=3). ***$p<0.001$; **$p<0.01$; *$p<0.05$. n.s.: differences were not statistically significant.

Appendix A. Supplementary data

Figure S1. Intercellular interactions in control MDA-MB-231 cells are promoted by Gal-8 in a dose- and glycan-dependent manner. Aggregation in control MDA-MB-231 and MDA-shControl cells was performed by incubating the cells with increasing concentrations of exogenous soluble rGal-8 (1-5 μM). Lactose (100 mM) was used as a saccharide inhibitor. Unless indicated, statistical significance was calculated compared to cells without lectin (rGal-8: 0 μM) and lactose treatment. ***$p<0.001$; **$p<0.01$; *$p<0.05$. Data are presented as mean values ±

ACCEPTED MANUSCRIPT

S.E.M., and were analyzed by two-way ANOVA with Tukey post-test (n=5). n.s.: differences were not statistically significant.

Table S1. Detailed structural characterization of N-glycan species present in ALCAM from MDA-MB-231 cells. Structure abbreviations: all N-glycans have two core GlcNAcs; F at the start of the abbreviation indicates a core fucose (CF) α(1-6)-linked to the inner GlcNAc; Mx, number (x) of mannose on core GlcNAcs; Ax, number of antennae (GlcNAc) on trimannosyl core; A2, biantennary with both GlcNAcs as β(1-2)-linked; A3, triantennary with a GlcNAc linked β(1-2) to both mannose and the third GlcNAc linked β(1-4) to the α(1-3) linked mannose; A4, GlcNAcs linked as A3 with additional GlcNAc β(1-6) linked to α(1-6) mannose; B, bisecting GlcNAc linked β(1-4) to β(1-3) mannose; Gx, number (x) of β(1-4) linked galactose on antenna; Sx, number (x) of sialic acids linked to galactose. Dx: isoforms with different high mannose (HM)-binding. Peaks calculated into specific features are highlighted in grey. The N-glycans shown are coloured according to their sialylation, *i.e.* red for neutral (N) N-glycans, blue for monosialylated (S1) structures, green for disialylated (S2) structures, purple for trisialylated (S3) structures and orange for tetrasialylated (S4) structures. Glycans were represented according to the symbol nomenclature proposed by [64].

ACCEPTED MANUSCRIPT

ACCEPTED MANUSCRIPT

Highlights

- ALCAM silencing decreases *in vitro* cell adhesion and migration onto Gal-8.
- Surface ALCAM establishes glycan-dependent cell interactions with Gal-8.
- Either Gal-8 or ALCAM silencing attenuates cell-cell aggregation.
- In mouse xenografts, Gal-8 and ALCAM silencing synergistically slow down tumor growth.

ACCEPTED MANUSCRIPT

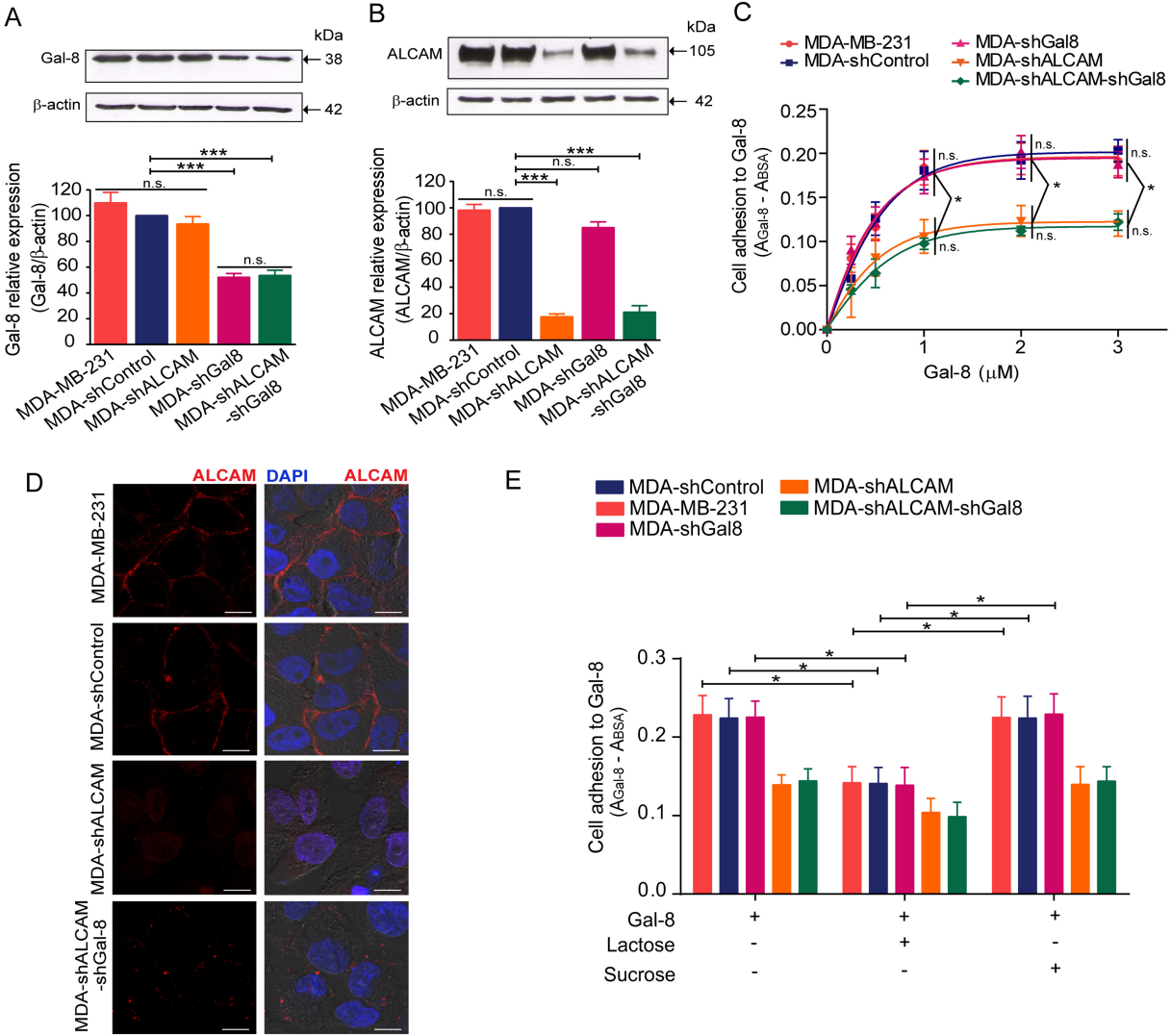
A
kDa
Gal-8
38
β-actin
42
***
***
n.s.
n.s.
Gal-8 relative expression
(Gal-8/β-actin)
120
100
80
60
40
20
0
MDA-MB-231
MDA-shControl
MDA-shALCAM
MDA-shGal8
MDA-shALCAM
-shGal8
B
kDa
ALCAM
105
β-actin
42
***
n.s.
***
n.s.
ALCAM relative expression
(ALCAM/β-actin)
120
100
80
60
40
20
0
MDA-MB-231
MDA-shControl
MDA-shALCAM
MDA-shGal8
MDA-shALCAM
-shGal8
C
MDA-MB-231
MDA-shControl
MDA-shGal8
MDA-shALCAM
MDA-shALCAM-shGal8
Cell adhesion to Gal-8
(AGal-8 - ABSA)
0.25
0.20
0.15
0.10
0.05
0.00
n.s.
n.s.
n.s.
n.s.
n.s.
n.s.
*
*
*
0
1
2
3
Gal-8 (μM)
D
ALCAM
DAPI
ALCAM
MDA-MB-231
MDA-shControl
MDA-shALCAM
MDA-shALCAM
-shGal-8
E
MDA-shControl
MDA-MB-231
MDA-shGal8
MDA-shALCAM
MDA-shALCAM-shGal8
Cell adhesion to Gal-8
(AGal-8 - ABSA)
0.3
0.2
0.1
0.0
*
*
*
*
*
*
Gal-8
Lactose
Sucrose
+
-
-
+
-
-
+
-
+

Figure 1

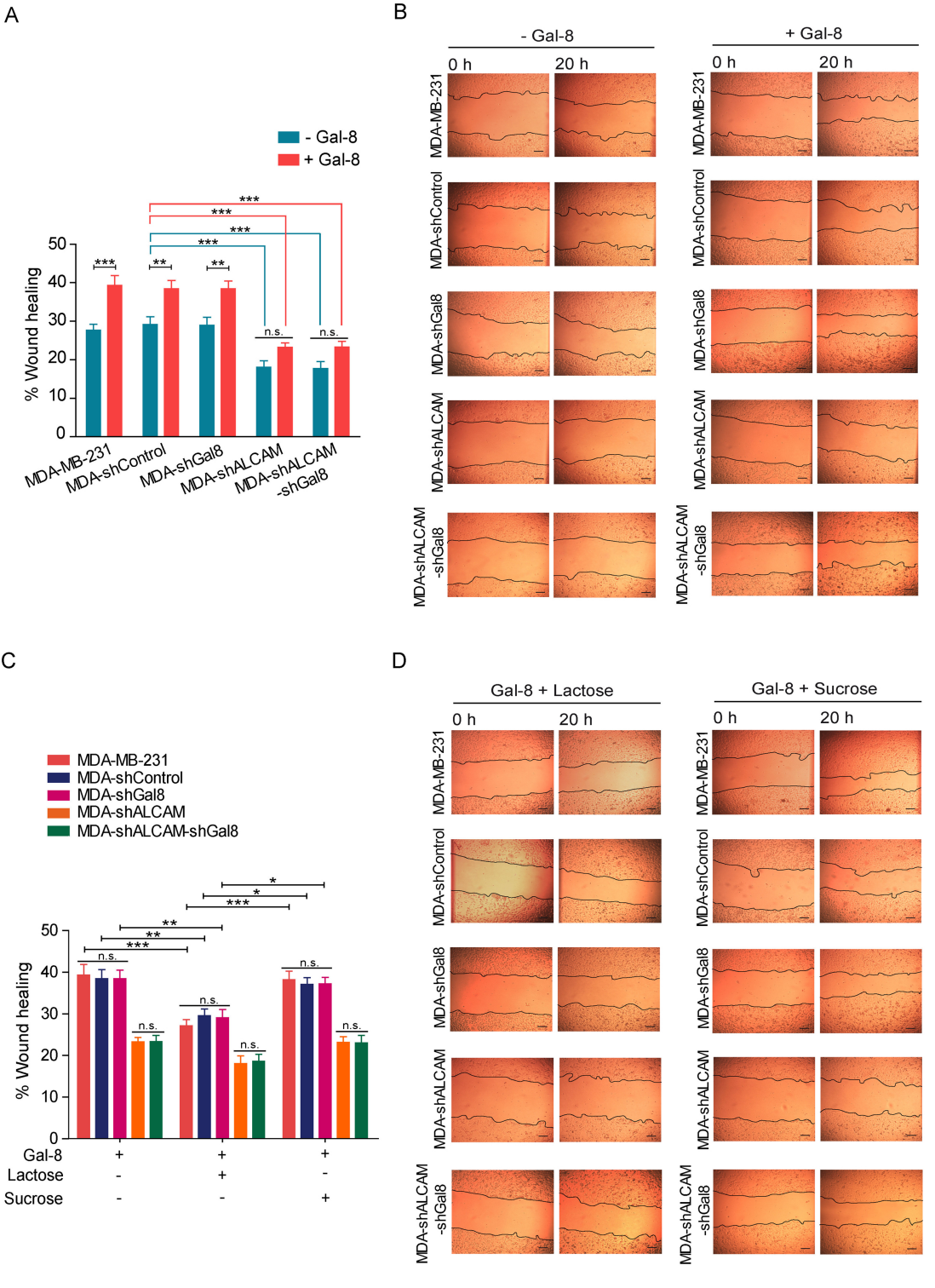
A
- Gal-8
+ Gal-8
% Wound healing
MDA-MB-231
MDA-shControl
MDA-shGal8
MDA-shALCAM
MDA-shALCAM -shGal8
n.s.
B
- Gal-8
+ Gal-8
0 h
20 h
C
Gal-8
Lactose
Sucrose
D
Gal-8 + Lactose
Gal-8 + Sucrose

Figure 2

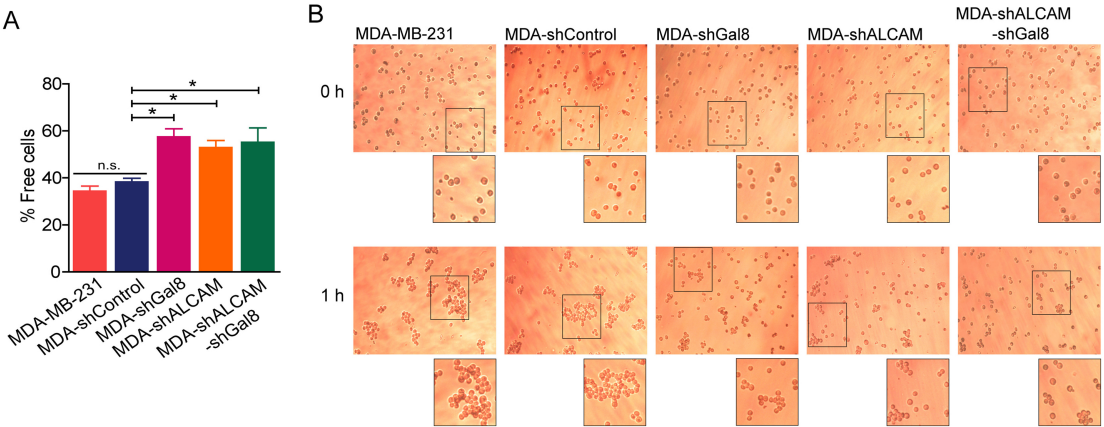
A
% Free cells
80
60
40
20
0
n.s.
*
*
*
MDA-MB-231
MDA-shControl
MDA-shGal8
MDA-shALCAM
MDA-shALCAM
-shGal8
B
MDA-MB-231
MDA-shControl
MDA-shGal8
MDA-shALCAM
MDA-shALCAM
-shGal8
0 h
1 h

Figure 3

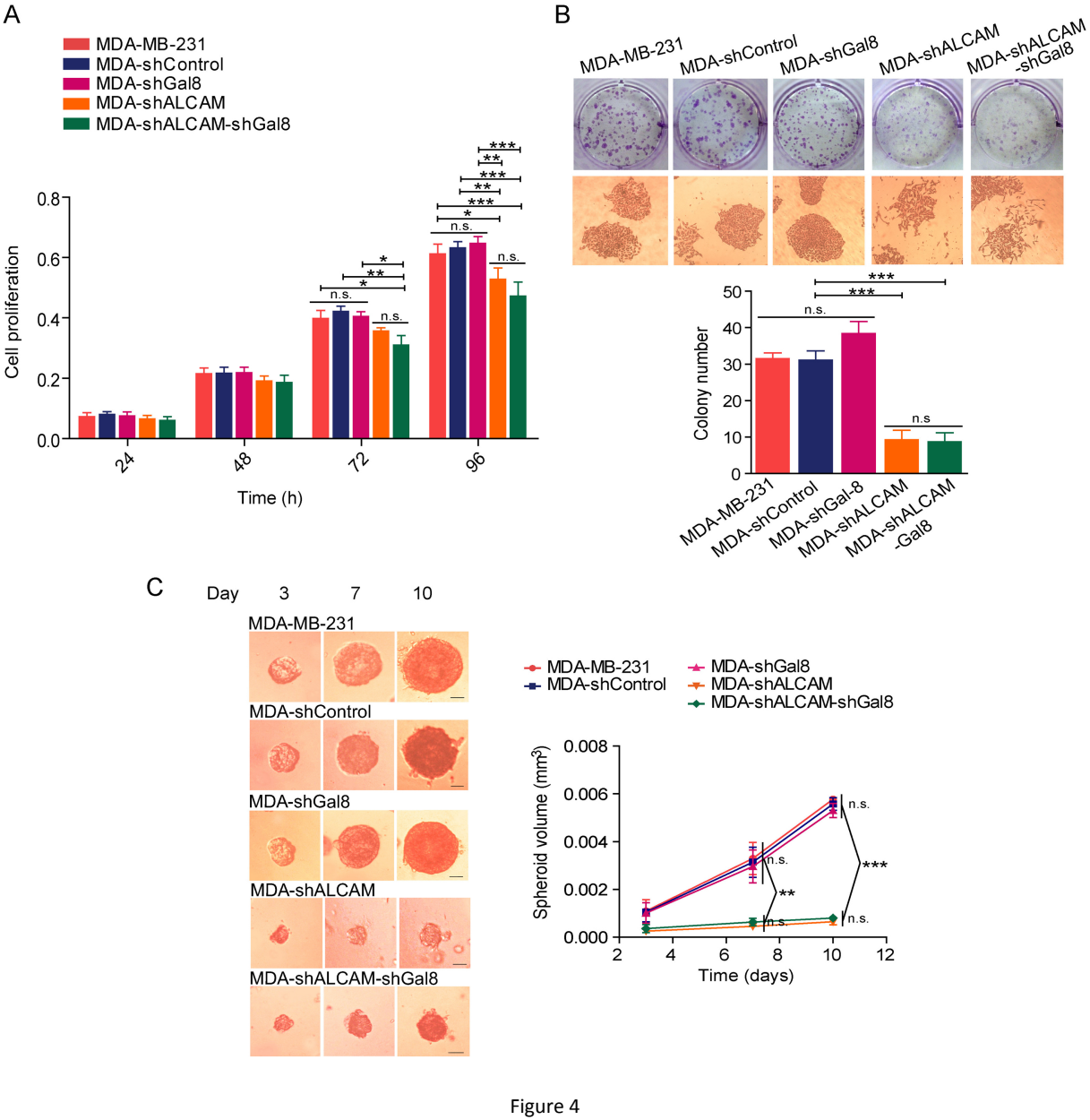
A
MDA-MB-231
MDA-shControl
MDA-shGal8
MDA-shALCAM
MDA-shALCAM-shGal8
Cell proliferation
Time (h)
24
48
72
96
B
MDA-MB-231
MDA-shControl
MDA-shGal8
MDA-shALCAM
MDA-shALCAM -shGal8
Colony number
C
Day 3 7 10
MDA-MB-231
MDA-shControl
MDA-shGal8
MDA-shALCAM
MDA-shALCAM-shGal8
Spheroid volume (mm3)
Time (days)

Figure 4

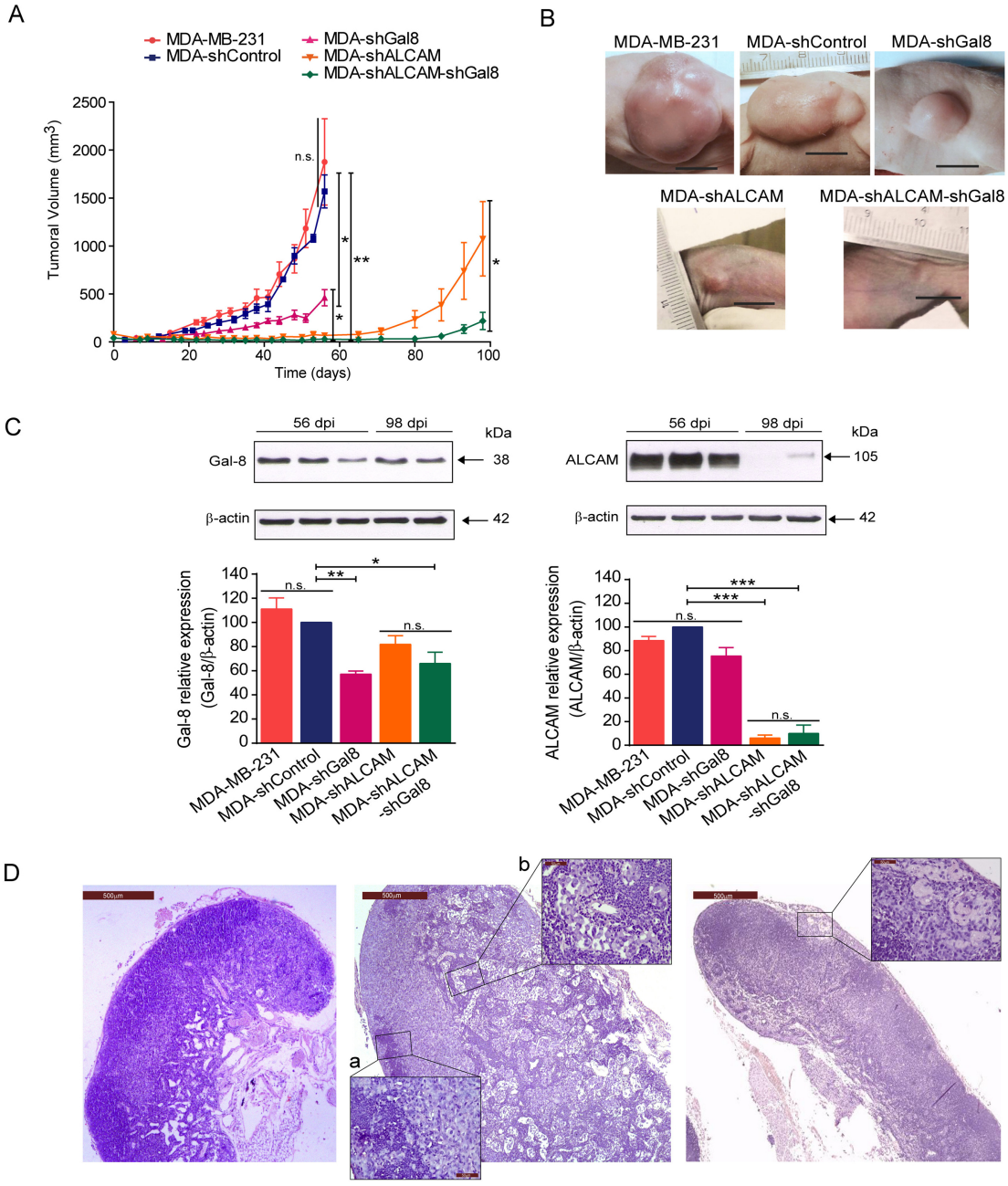
A
MDA-MB-231
MDA-shControl
MDA-shGal8
MDA-shALCAM
MDA-shALCAM-shGal8
Tumoral Volume (mm3)
Time (days)
n.s.
*
**
B
MDA-MB-231
MDA-shControl
MDA-shGal8
MDA-shALCAM
MDA-shALCAM-shGal8
C
56 dpi
98 dpi
kDa
Gal-8
38
β-actin
42
ALCAM
105
Gal-8 relative expression (Gal-8/β-actin)
ALCAM relative expression (ALCAM/β-actin)
***
D
a
b
500µm

Figure 5

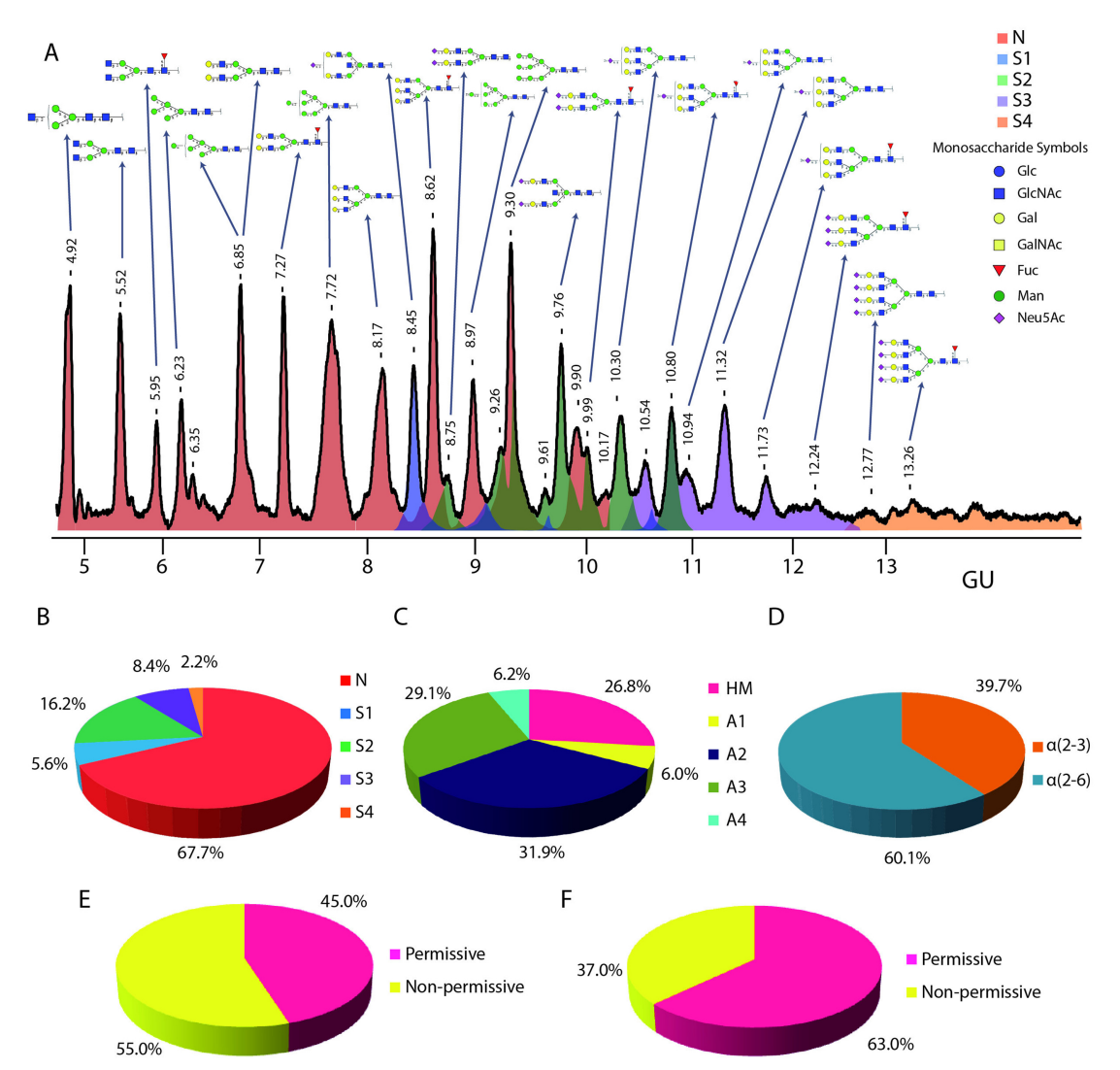
A
N
S1
S2
S3
S4
Monosaccharide Symbols
Glc
GlcNAc
Gal
GalNAc
Fuc
Man
Neu5Ac
4.92
5.52
5.95
6.23
6.35
6.85
7.27
7.72
8.17
8.45
8.62
8.75
8.97
9.26
9.30
9.61
9.76
9.90
9.99
10.17
10.30
10.54
10.80
10.94
11.32
11.73
12.24
12.77
13.26
5
6
7
8
9
10
11
12
13
GU
B
8.4%
2.2%
16.2%
5.6%
67.7%
N
S1
S2
S3
S4
C
6.2%
29.1%
26.8%
6.0%
31.9%
HM
A1
A2
A3
A4
D
39.7%
60.1%
α(2-3)
α(2-6)
E
45.0%
55.0%
Permissive
Non-permissive
F
37.0%
63.0%
Permissive
Non-permissive

Figure 6

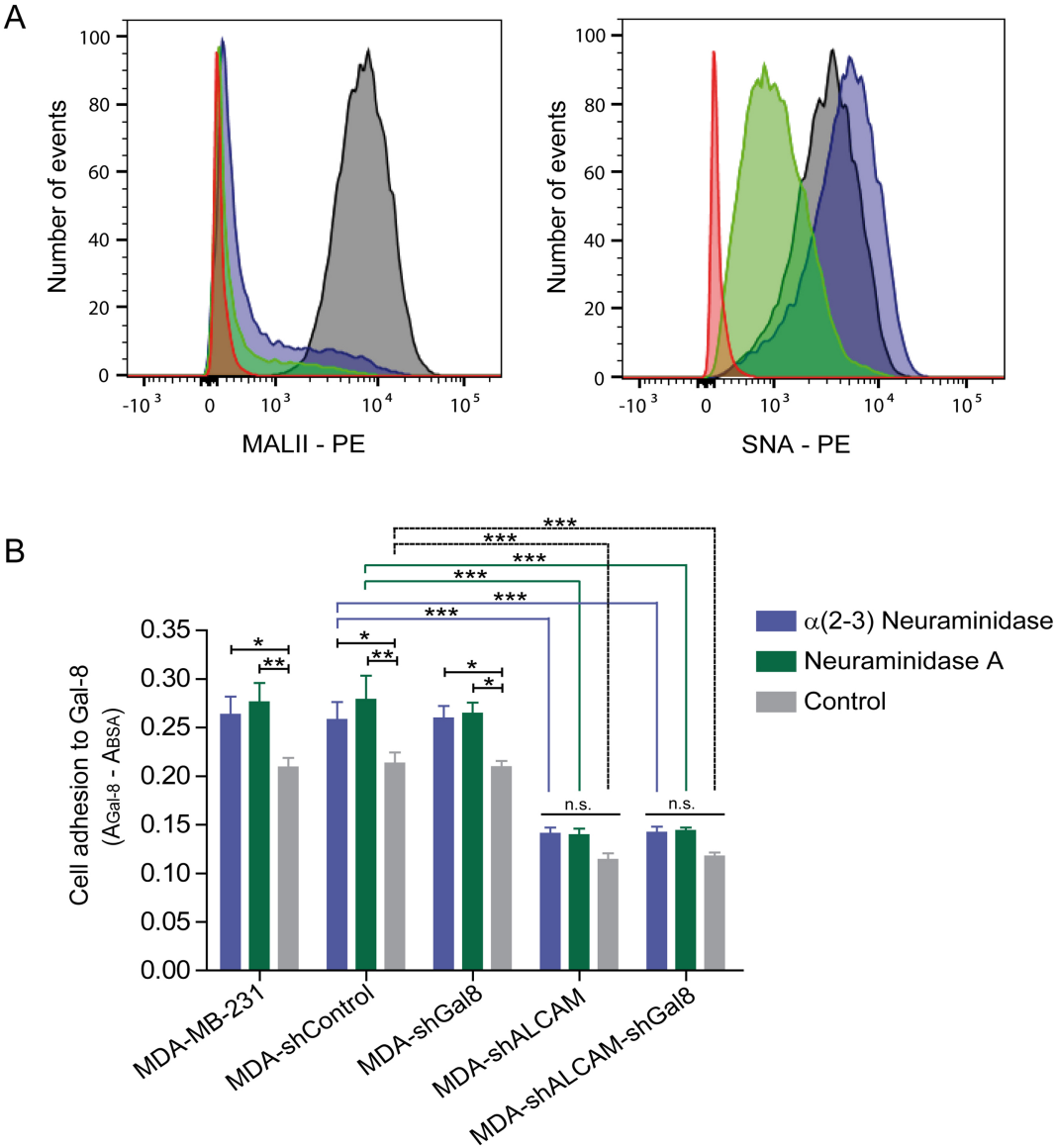
A
Number of events
MALII - PE
SNA - PE
B
Cell adhesion to Gal-8
(AGal-8 - ABSA)
α(2-3) Neuraminidase
Neuraminidase A
Control
n.s.
MDA-MB-231
MDA-shControl
MDA-shGal8
MDA-shALCAM
MDA-shALCAM-shGal8

Figure 7

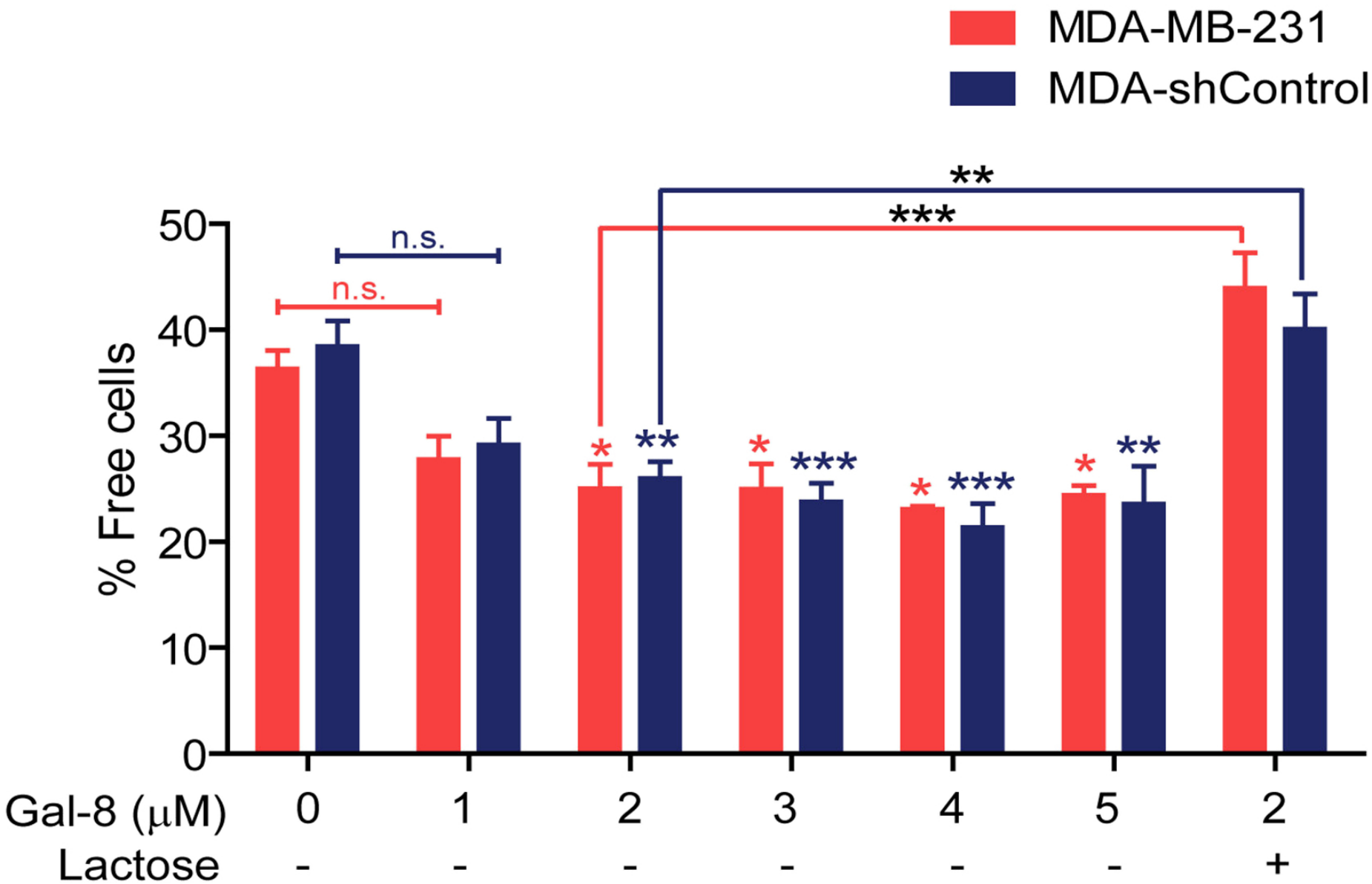
MDA-MB-231
MDA-shControl
% Free cells
50
40
30
20
10
0
n.s.
n.s.
**
***
*
**
*
***
*
***
*
**
*
**
Gal-8 (μM)
0
1
2
3
4
5
2
Lactose
-
-
-
-
-
-
+

Figure 8